Mitochondrial Aurora kinase A induces mitophagy by interacting with MAP1LC3 and Prohibitin 2.

Giulia Bertolin[1,#,§], Marie-Clotilde Alves-Guerra[2], Agnès Burel[3], Claude Prigent[1], Roland Le Borgne[1] and Marc Tramier[1].

[1] Univ Rennes, CNRS, IGDR (Genetics and Development Institute of Rennes), UMR 6290, F-35000 Rennes, France
[2] Université de Paris, Institut Cochin, INSERM, CNRS F-75014 Paris, France
[3] Univ Rennes, MRic CNRS, INSERM, SFR Biosit, UMS 3480, F-35000 Rennes, France

[#] Lead contact

[§] Correspondence and requests for materials should be addressed to G.B. (giulia.bertolin@univ-rennes1.fr; Tel: +330223237516)

Abstract

Epithelial and haematologic tumours often show the overexpression of the serine/threonine kinase AURKA. Recently, AURKA was shown to localise at mitochondria, where it regulates mitochondrial dynamics and ATP production. Here we define the molecular mechanisms of AURKA in regulating mitochondrial turnover by mitophagy. When overexpressed, AURKA induces the rupture of the Outer Mitochondrial Membrane in a proteasome-dependent manner. Then, AURKA triggers the degradation of Inner Mitochondrial Membrane (IMM)/matrix proteins by interacting with core components of the autophagy pathway. On the IMM, the kinase forms a tripartite complex with MAP1LC3 and the mitophagy receptor PHB2. This complex is necessary to trigger mitophagy in a PARK2/Parkin-independent manner. The formation of the tripartite complex is induced by the phosphorylation of PHB2 on Ser39, which is required for MAP1LC3 to interact with PHB2. Last, treatment with the PHB2 ligand Xanthohumol blocks AURKA-induced mitophagy by destabilising the tripartite complex. This treatment also restores normal ATP production levels. Altogether, these data provide evidence for a previously undetected role of AURKA in promoting mitophagy through the interaction with PHB2 and MAP1LC3. This work paves the way to the use of function-specific pharmacological inhibitors to counteract the effects of the overexpression of AURKA in cancer.

Keywords: AURKA, mitophagy, PHB2, MAP1LC3, tripartite complex, Xanthohumol

Introduction

AURKA is a serine/threonine kinase with multiple functions during interphase and cell division. It is frequently overexpressed in solid tumours and during haematological malignancies, where it correlates with poor patient survival and resistance to treatments (Bertolin and Tramier, 2019; Farag, 2011; Nikonova et al., 2013). AURKA was originally found at centrosomes and at the mitotic spindle in *Xenopus laevis*, (Andrésson and Ruderman, 1998; Glover et al., 1995; Paris and Philippe, 1990; Roghi et al., 1998) and in *Drosophila melanogaster* (Giet et al., 2002; Lee et al., 2006; Wang et al., 2006; Wirtz-Peitz et al., 2008). AURKA was then reported to localise to other subcellular locations such as the nucleus (Zheng et al., 2016), primary cilia (Kinzel et al., 2010; Lee et al., 2012; Mergen et al., 2013; Pugacheva and Golemis, 2005; Pugacheva et al., 2007), and more recently at mitochondria (Bertolin et al., 2018; Grant et al., 2018). At this compartment, we and others reported that AURKA regulates two key mitochondrial functions as organelle dynamics and ATP production throughout the cell cycle (Bertolin et al., 2018; Grant et al., 2018; Kashatus et al., 2011). Given these multiple locations, our knowledge of the subcellular interactome of AURKA and the new intracellular functions for this kinase is constantly growing (Bertolin and Tramier, 2019).

Mitochondria are dynamic organelles continuously undergoing cycles of fusion and fission to meet the energy requirements of the cell (Mishra and Chan, 2016). Concomitantly to these functions, turnover programs are also activated to selectively eliminate defective portions of the mitochondrial network. These programs mainly rely on mitochondrial-specific autophagy (mitophagy), and they are necessary for cell homeostasis in both physiological and pathological paradigms (Pickrell and Youle, 2015). The mitophagy pathway has been

extensively characterised in paradigms of Parkinson's disease (PD). The PD-linked proteins PARK2-Parkin and PTEN-induced kinase 1 (PINK1) directly interact with various components of the autophagy machinery, and constitute a common pathway triggering mitochondrial turnover (Youle and Narendra, 2011). Downstream of PARK2-Parkin and PINK1, the molecular actors regulating organelle-specific elimination pathways like mitophagy are key components of the autophagy pathway. Upon the induction of mitophagy, a family of small ubiquitin-like modifiers - MAP1LC3 and GABARAP proteins - are modified through the addition of a phosphatidylethanolamine molecule (Nakatogawa, 2013). This modification hallmarks for the activation of MAP1LC3 on the nascent autophagosomal membrane (Mercer et al., 2018). Together with MAP1LC3 lipidation, the serine/threonine kinase UNC-51-like kinase 1 (ULK1) and ATG9 proteins independently contribute to the early steps of autophagosome formation during mitophagy (Hurley and Young, 2017). Organelle-specific autophagy then employs selective downstream adaptors and effectors such as Sequestosome-1 (SQSTN1/p62) (Geisler et al., 2010), neighbour of BRCA1 gene 1 (NBR1) (Isakson et al., 2013), nuclear dot-protein 52 (NDP52) and Optineurin (OPTN) (Lazarou et al., 2015), which are recruited to defective mitochondria and are necessary for their consequent elimination within autophagosomes.

Although less extensively characterised, physiological paradigms for mitophagy exist in specific cell types. For instance, the Outer Mitochondrial Membrane (OMM) protein Nip3-like protein X (NIX) interacts with MAP1LC3 and its homologue GABARAP to trigger the elimination of mitochondria in red blood cells (Kim et al., 2007; Mortensen et al., 2010; Novak et al., 2010; Schwarten et al., 2009; Zhang et al., 2009). More recently, Prohibitin 2 (PHB2) was identified as the receptor of MAP1LC3 on the Inner Mitochondrial Membrane (IMM) (Wei et al., 2017). In the same study using *C. elegans*, PHB2 was shown to be essential both in PARK2-Parkin/PINK1-dependent mitophagy in cultured cells and for the clearance of paternal organelles upon fertilisation, a physiological paradigm of mitochondrial turnover.

We here discover that overexpressed AURKA triggers mitophagy by forming a tripartite complex with MAP1LC3 and PHB2 at mitochondria. AURKA induces organelle turnover independently of PARK2/Parkin. Last, we identify a the PHB2 ligand Xanthohumol as a potential pharmacological strategy to block mitophagy by destabilising the tripartite complex in cells overexpressing AURKA. While the overexpression of AURKA exacerbates mitochondrial ATP production (Bertolin et al., 2018), Xanthohumol restores normal ATP levels in cells, further corroborating the link between mitophagy and mitochondrial energy production.

Results

Overexpressed AURKA triggers the recruitment of MAP1LC3 to mitochondria and it induces mitochondrial mass loss.

We previously reported that AURKA elongates the mitochondrial network when overexpressed (Bertolin et al., 2018). Under the same experimental conditions, we detected a partial loss of mitochondrial mass in MCF7 cells – an epithelial breast cancer cell line – (Fig. 1A), when measuring the area covered by the mitochondrial matrix marker PMPCB (Bertolin et al., 2013). To evaluate whether PMPCB loss is directly linked to the localisation of AURKA at mitochondria, we overexpressed the cytosolic-only AURKA variant ΔNter. As previously reported, this construct lacks the mitochondrial-targeting sequence of AURKA (Bertolin et al., 2018). Conversely to the normal protein, AURKA ΔNter did not induce any loss of mitochondrial mass (Fig. 1A). Interestingly, no mitochondrial mass loss was observed when endogenous AURKA was depleted by siRNA (Fig. 1A). To further validate the loss of mitochondrial mass observed in cells overexpressing AURKA, we used two additional approaches: the analysis of mitochondrial protein abundance by western blotting, and flow cytometry analyses of mitochondrial mass. Biochemical analyses were carried out in HEK293 cells, a mitochondria-rich cell model previously used to characterise the presence and the functions of AURKA at mitochondria (Bertolin et al., 2018). In western blotting analyses of total protein fractions, we monitored the abundance of the OMM protein TOMM22 and of the IMM protein TIMM50. Consistent with confocal microscopy data, a significant loss of both markers was observed in cells overexpressing AURKA (Fig. 1B). Similarly, we evaluated the loss of mitochondrial mass by flow cytometry taking advantage of the polarisation-insensitive dye MitoTracker Green. When overexpressing AURKA in HEK293 cells, the mean fluorescence intensity of MitoTracker Green decreased by nearly 50% (Fig. 1C). Concomitantly with a decrease in MitoTracker Green fluorescence intensity, the polarisation-sensitive dye TMRM failed to accumulate at mitochondria under these conditions (Supplementary Fig. 1A). This indicates that mitochondria of cells overexpressing AURKA undergo a loss of mitochondrial membrane potential.

As the loss of mitochondrial mass is commonly associated with the autophagic elimination of mitochondria – mitophagy – (Klionsky et al., 2016), we wanted to explore whether AURKA plays a role in this turnover pathway. We first monitored the activation of the autophagic marker MAP1LC3 in

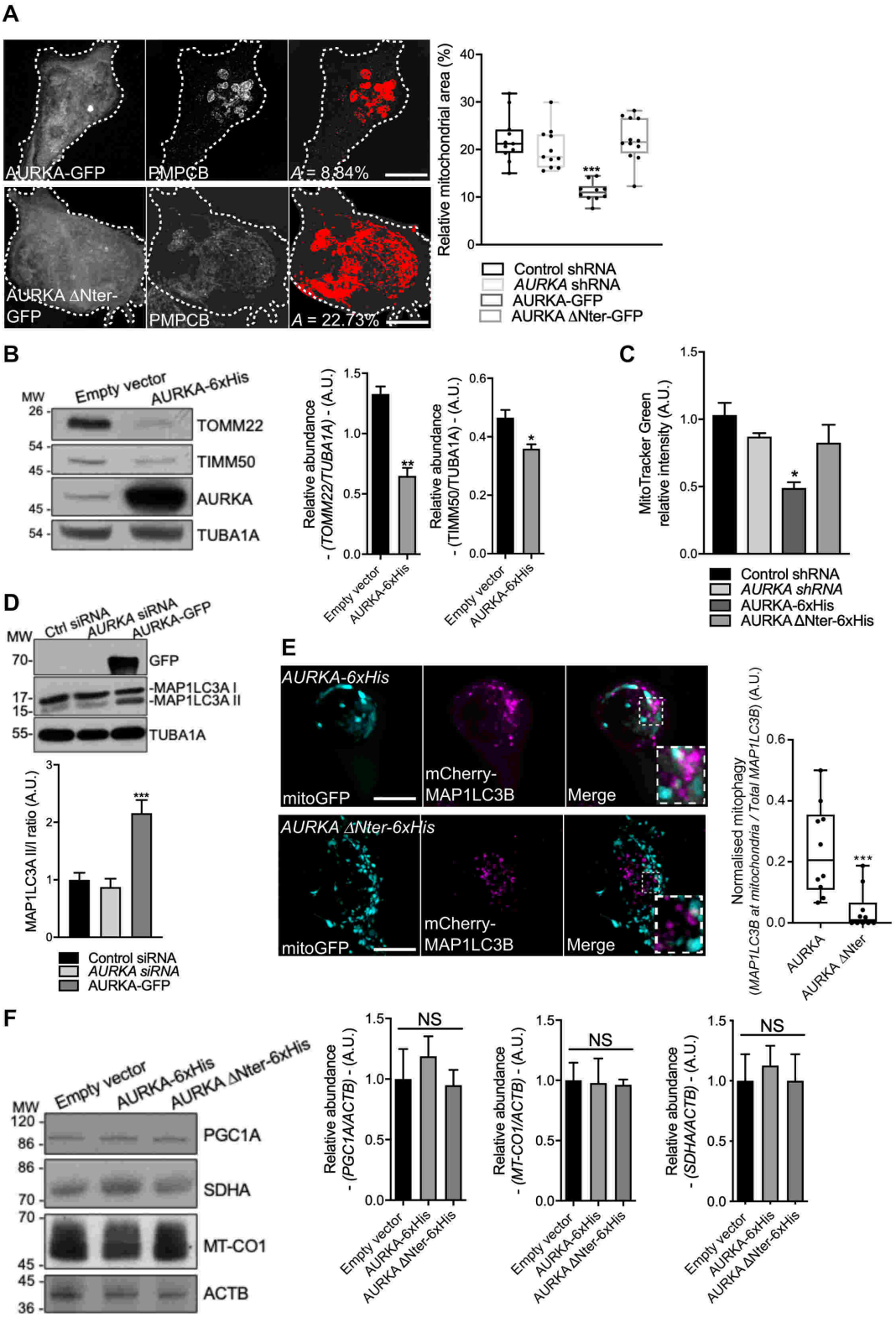

Figure 1. Mitochondria are eliminated by mitophagy in cells overexpressing AURKA. (A) Loss of PMPCB staining (threshold mask and corresponding quantification) in MCF7 cells transfected with AURKA-GFP or AURKA ΔNter-GFP. *A*=mitochondrial area normalised against total cell area (%). *n*=10 cells per condition from one representative experiment (of three). (B) Representative immunoblot and quantification of the normalised abundance of the OMM marker TOMM22 and of the IMM marker TIMM50 in total lysates of HEK293 cells transfected as indicated. Loading control: TUBA1A. *n*=3 independent experiments. (C) Relative MitoTracker Green FM fluorescence measured by flow cytometry on HEK293 cells transfected as indicated. *n*=3 independent experiments with at least 30,000 cells per condition quantified. (D) Representative immunoblot of the autophagy marker MAP1LC3 and quantification of the MAP1LC3 II/I ratio in total lysates of HEK293 cells transfected as indicated. *n*=3 independent experiments. (E) (Left) Immunofluorescence micrographs of MCF7 cells overexpressing AURKA 6xHis (top panels) or AURKA ΔNter-6xHis (bottom panels), and transfected with a mitochondrially-targeted GFP (mitoGFP) and mCherry-MAP1LC3B constructs. Inset: higher magnification of the dotted area. (Right) Corresponding colocalisation coefficient between mitoGFP and mCherry-MAP1LC3B. *n*=10 cells per condition from one representative experiment (of three). (F) Representative immunoblot and quantification of the normalised abundance of the mitochondrial biogenesis factors PGC1A, MT-CO1 and SDHA in total lysates of HEK293 cells transfected as indicated. Loading control: ACTB. *n*=3 independent experiments. Scale bar: 10µm. Data represent means ± s.e.m, unless in (A, C) where they extend from min to max. **P*<0.05, ***P*<0.01, ****P*<0.001 compared to the corresponding 'Control' (A, B, E), 'AURKA' (C), or 'Empty vector' conditions (D, F). NS: not significant. A.U.: arbitrary units.

HEK293 cells. Measured as the conversion of MAP1LC3 I into II, this modification is a commonly used readout to assess activation of autophagy (Klionsky et al., 2016). We observed an increase in MAP1LC3II only when AURKA was overexpressed (Fig. 1D). However, we sought to determine whether MAP1LC3 activation was a sign of bulk autophagy or of mitophagy. Using confocal microscopy, we evaluated the proportion of mitochondria colocalising with MAP1LC3-positive vesicles in MCF7 cells. The proximity of mitochondria and MAP1LC3 was observed upon the overexpression of AURKA, but not in the presence of AURKA ΔNter (Fig. 1E). We further confirmed these results in the fruit fly, a model that allows the comparison of the effects of a physiological expression of AURKA to its loss-of-function or gain-of-function. We quantified the number of Atg8 dots, the fly orthologue of MAP1LC3, juxtaposed to mitoGFP-positive mitochondria, and normalised to the total number of Atg8 dots (Supplementary Fig. 1B). Quantifications were carried out in the fly notum, a monolayer of epithelial cells. Again, we observed an increased number of Atg8 dots on mitochondria only when AURKA was overexpressed, and this was not observed in any other condition.

Last, we also evaluated whether a loss in mitochondrial mass is correlated with a concomitant alteration of mitochondrial biogenesis. The relative abundance of biogenesis-related proteins as the mitochondrially-encoded COXI subunit (MT-CO1), the nuclearly-encoded SDHA protein or the PGC1A transcription factor was not altered in cells overexpressing AURKA compared to cells transfected with an empty vector or AURKA ΔNter (Fig. 1F). Therefore, the presence of overexpressed AURKA seems not to have an impact on mitochondrial biogenesis.

These data indicate that the overexpression of AURKA induces the recruitment of MAP1LC3 to mitochondria, together with mitochondrial depolarisation and a loss of mitochondrial mass.

AURKA overexpression leads to lysosomal accumulation and to the activation of mitophagy.

As our results indicate the presence of mitophagy-related features in cells overexpressing AURKA, we then used Transmission Electron Microscopy to better visualise this turnover. In HEK293 cells subjected to TEM analyses after the overexpression of AURKA, we observed that lysosomes were more abundant than in control cells or in cells where the kinase was silenced (Fig. 2A). A nearly twofold increase in the lysosomal content was confirmed in live HEK293 cells incubated with LysoTracker Red, a fluorescent probe used to measure lysosomal mass (Fig. 2B). This The overexpression of the cytosolic-only AURKA ΔNter variant did not affect lysosomal mass. In addition, TEM images revealed that lysosomes (Fig. 2A, right panel, magenta arrows) were proximal to fragmented mitochondria (*m*), which are known to be preferential targets for degradation by mitophagy (Twig and Shirihai, 2011).

We then evaluated whether this increase in lysosomal content was a mere accumulation, or one of the readouts of activated, mitochondrial-related autophagy. To this end, we evaluated the red/green fluorescence ratio of a mitochondrially-targeted GFP-mCherry tandem (hereby, mitoTandem). This tool relies on the quenching of the GFP fluorophore inside lysosomes due to their acidic pH, while the mCherry fluorophore is insensitive to the pH properties of the surrounding environment. mitoTandem has previously been used to estimate the presence of mitochondrial-related autophagy (Princely Abudu et al., 2019). In control cells not overexpressing AURKA or in cells overexpressing AURKA ΔNter, the mCherry/GFP integrated density ratio was close to 1, indicating no significant differences in the fluorescence intensities of both fluorophores (Supplementary Fig. 2A). Conversely, the mCherry/GFP ratio was increased in the presence of overexpressed AURKA, potentially due to the quenching of GFP in an acidic environment and suggesting the presence of mitochondria-related autophagy.

To further verify the activation of mitophagy in cells overexpressing AURKA, we investigated whether AURKA directly interacts with selective components of the autophagic pathway, providing a potentially direct link to the loss of mitochondrial mass and the increase in the number of lysosomes in AURKA-overexpressing cells. To search for weak and/or potentially transient protein-protein interactions between AURKA and the molecular players of autophagy, we used Förster's Resonance Energy Transfer (FRET)/Fluorescence Lifetime Imaging Microscopy (FLIM) (Leray et al., 2013; Padilla-Parra et al., 2008). FRET was represented as ΔLifetime, which is the net difference between the lifetime of the donor-only construct and the donor in the presence of the acceptor. A positive ΔLifetime is indicative of FRET, and therefore of a physical interaction between two proteins. We previously used ΔLifetime as a convenient way to illustrate molecular interactions (Bertolin et al., 2019). FRET/FLIM analyses revealed that overexpressed AURKA is in close proximity (< 10 nm, consistent with molecular interactions) with MAP1LC3 and with the lysosomal protein LAMP1 in MCF7 cells (Fig. 2C). To corroborate FRET/FLIM analyses, we used the fluorescent mCherry-GFP MAP1LC3 tandem to follow autophagosomal maturation in cells overexpressing AURKA (Tresse et al., 2010).

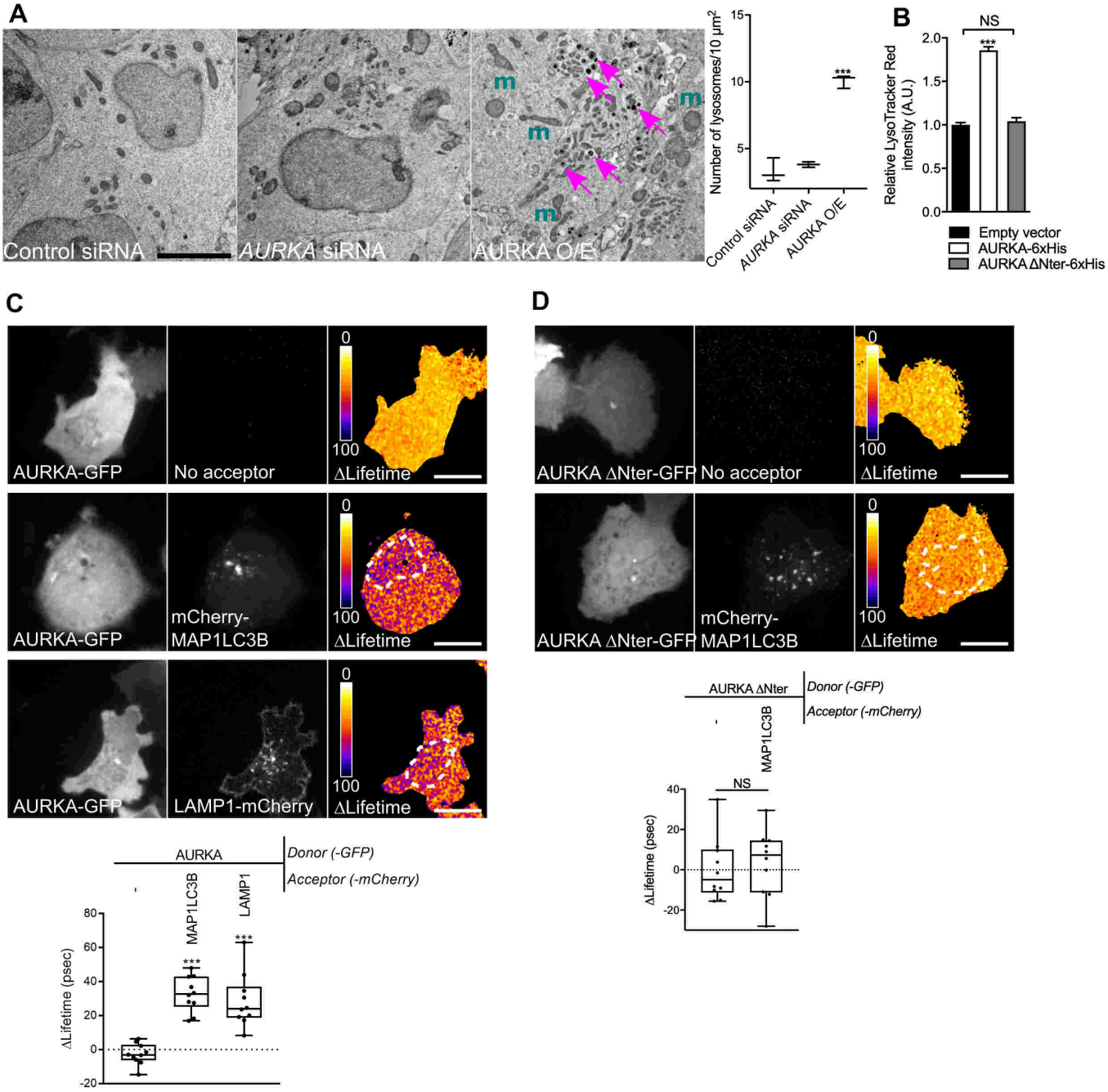

Figure 2. The autophagic machinery is activated and it interacts with overexpressed AURKA. (A) (Left) HEK293 cells imaged by transmission electron microscopy (TEM). Cells were transfected with control- or *AURKA*-specific siRNAs, or with an AURKA-GFP vector (AURKA O/E). m = mitochondria; rmagenta arrows = lysosomes. (Right) Quantification of lysosomal number per 10 µm^2 of cell surface. *n* = 20 images per condition from two independent experiments. Scale bar: 1 µm. (B) Relative LysoTracker Red fluorescence measured by flow cytometry on HEK293 cells transfected as indicated. *n*=3 independent experiments with at least 30,000 cells per condition quantified. Data represent means ± s.e.m, A.U.: arbitrary units. (C-D) FRET by FLIM analyses on MCF7 cells expressing AURKA-GFP (C) or AURKA ΔNter-GFP (D) alone or together with mCherry-MAP1LC3B or LAMP1-mCherry. Dotted area: autophagosome/autolysosome-rich areas Pseudocolour scale: pixel-by-pixel ΔLifetime. (Lower panels) Corresponding ΔLifetime quantifications in the dotted area. *n*=10 cells per condition of one representative experiment (of three). Data extend from min to max, unless where indicated. Scale bar: 10 µm. ***P < 0.001 against the 'Control siRNA' (A), the 'Empty vector' (B) or the 'AURKA- No acceptor' (C, D) conditions. NS: not significant.

Similarly to mitoTandem, yellow MAP1LC3 puncta indicate the presence of autophagosomes in a non-acidic environment, whereas mCherry-only puncta are the consequence of GFP quenching and indicate the presence of autolysosomes. In cells overexpressing AURKA, both autophagosomes and autolysosomes were present (Supplementary Fig. 2B), substantiating the capacity of AURKA to interact with early (MAP1LC3) and late (LAMP1) markers of the autophagic pathway (Fig. 2C). On the contrary, the overexpression of the cytosolic-only AURKA ΔNter did not lead to a massive autophagosomal nor autolysosomal activation (Supplementary Fig. 2B). Accordingly, no interaction of AURKA ΔNter with MAP1LC3 was detected by FRET/FLIM (Fig. 2D). This indicates that AURKA must be imported into mitochondria (Bertolin et al., 2018; Grant et al., 2018) and potentially processed into this compartment to come into contact with autophagic markers during the process of mitochondrial elimination.

The overexpression of AURKA independently induces proteasome-dependent OMM rupture and autophagy-dependent IMM digestion.

During mitophagy, mitochondrial elimination requires the proteasome-dependent degradation of the OMM (Chan et al., 2011; Di Rita et al., 2018; Wei et al., 2017; Yoshii et al., 2011). We thus explored whether the loss of mitochondrial mass occurring in MCF7 cells overexpressing AURKA requires OMM rupture, by monitoring the disappearance of the OMM marker TOMM22 in the presence or absence of the proteasomal inhibitor MG132. In immunofluorescence analyses, TOMM22 levels significantly decreased in cells overexpressing AURKA (Fig. 3A, upper panel), and the treatment with MG132 rescued its loss of (Fig. 3A, lower panel). We obtained similar results using western blotting and monitoring another OMM marker – MFN2 – (Fig. 3B). This suggests that the OMM is ruptured in a proteasome-dependent manner when AURKA is overexpressed.

The elimination of IMM proteins was previously shown to depend on the autophagy machinery (Yoshii et al., 2011). We then explored whether the mitochondrial innermost compartments undergo elimination through the autophagy pathway in AURKA-overexpressing cells. To this end, we used immunofluorescence approaches to quantify the loss of PMPCB, in cells overexpressing AURKA and in the presence or absence of the early autophagic inhibitor 3-methyladenine, or of the late autophagic inhibitor Bafilomycin A (Fig. 3C). Both inhibitors rescued the loss of PMPCB staining observed in cells treated with DMSO, as the mitochondrial mass observed in the presence of these two compounds is similar to the one of cells transfected with a control vector and not showing signs of mitochondrial loss. Again, similar results were obtained using western blotting approaches and with another IMM marker – TIMM50 – (Fig. 3B). We also noticed the existence of PMPCB-positive/TOM22-negative mitochondria in cells overexpressing AURKA (Fig. 3D), but not in cells expressing an AURKA ΔNter construct. These observations further suggest that the degradation of the OMM occurs prior to the digestion of the IMM/matrix compartments.

We then explored whether OMM rupture is necessary for the elimination of IMM/matrix markers. The loss of PMPCB and of TIMM50 were not restored when cells overexpressing AURKA were treated with MG132 (Fig. 3B and Supplementary Fig. 3A). This indicates that OMM rupture is not required for IMM/matrix degradation. As an additional way to explore whether AURKA-dependent IMM/matrix loss requires the activity of the proteasome, we analysed whether AURKA is still capable of interacting with MAP1LC3 upon proteasome inhibition. When OMM rupture is prevented by the addition of MG132, AURKA and MAP1LC3 still show a positive ΔLifetime in FRET/FLIM analyses (Fig. 3E). This was not due to a side-effect of MG132, as the addition of the drug did not modify the lifetime of AURKA-GFP in the absence of the acceptor (Supplementary Fig. 3B). Therefore, our results indicate that AURKA and MAP1LC3 interact in a comparable manner in the presence and in the absence of the OMM. Furthermore, we observed that the elimination of the OMM proteins TOMM22 and MFN2 did not require the autophagy degradation system (Fig. 3B and Supplementary Fig. 3C). This further supports the dissociation of OMM and IMM/matrix degradation pathways in AURKA-overexpressing cells.

Overall, our data dissociate the degradation pathways of the OMM and of the IMM/matrix components upon the overexpression of AURKA, and they indicate that this experimental paradigm recapitulates two features observed in other paradigms of mitophagy: proteasome-dependent OMM rupture and autophagy-dependent IMM/matrix degradation. We also provide evidence that OMM rupture is not a prerequisite for AURKA-dependent mitochondrial mass loss.

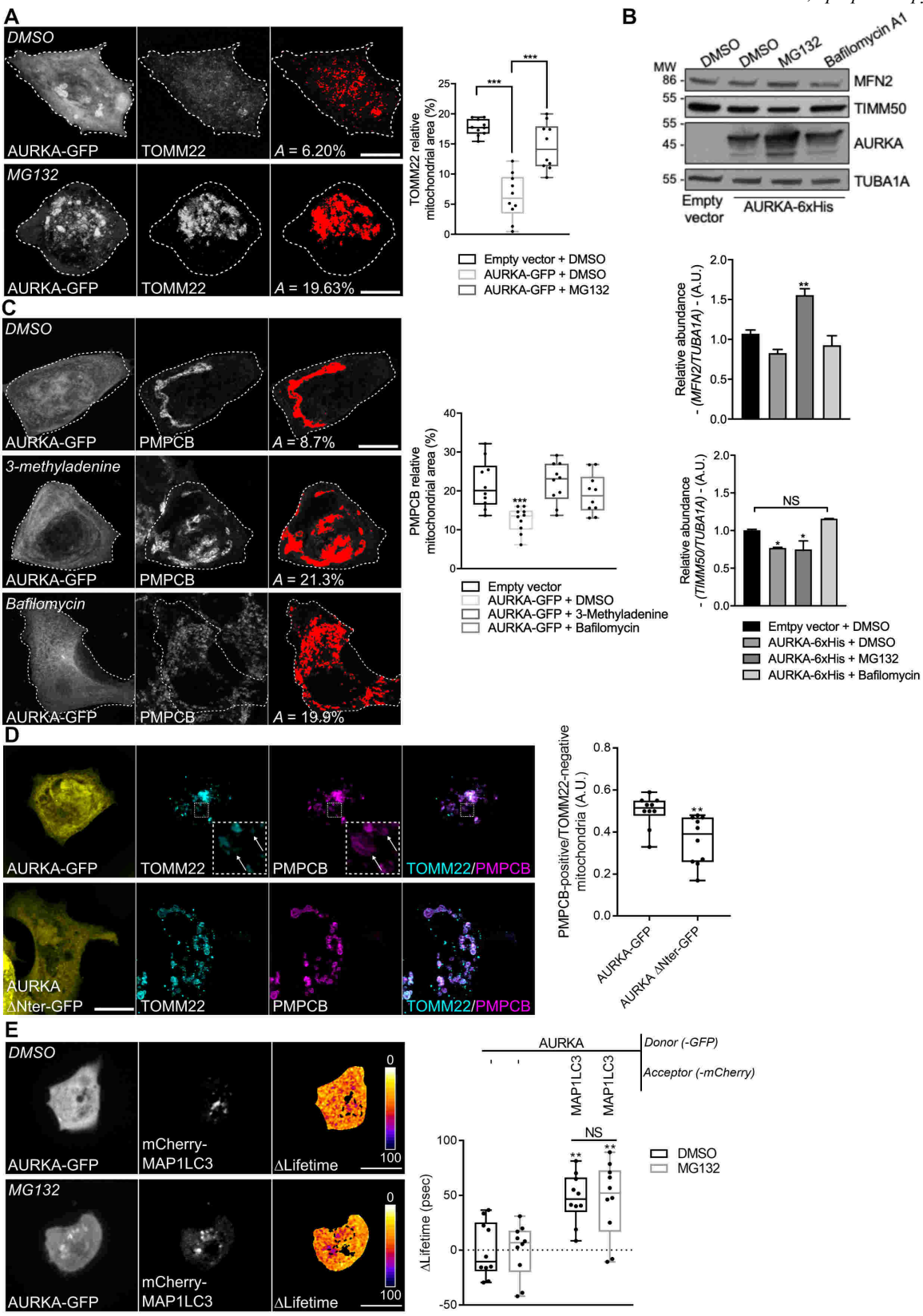

Figure 3. The OMM is ruptured in a proteasome-dependent manner when AURKA is overexpressed. (A) Loss of TOMM22 staining (threshold mask and corresponding quantification) in MCF7 cells transfected with an empty vector or with AURKA-GFP, and treated with DMSO or with the proteasome inhibitor MG132. (B) Representative immunoblot and quantification of the normalised abundance of the OMM marker MFN2 and of the IMM marker TIMM50 in total lysates of HEK293 cells transfected with AURKA-6xHis or an empty vector, and treated as indicated. Loading control: TUBA1A. *n*=3 independent experiments. (C) Loss of PMPCB staining (threshold mask and corresponding quantification) in MCF7 cells transfected with as indicated, and treated with DMSO or with autophagy inhibitors 3-methyladenine (3-MA) or Bafilomycin A1. (D) Representative micrographs and corresponding analyses of MCF7 cells transfected with AURKA-GFP or AURKA ΔNter-GFP and co-stained for TOMM22 and PMPCB. Insets: higher magnification of the dotted area. Arrows and quantification: TOMM22-negative/PMPCB-positive mitochondria. AURKA, TOMM22 and PMPCB were pseudocoloured yellow, cyan and magenta, respectively. (E) FRET by FLIM analyses on MCF7 cells expressing AURKA-GFP alone or together with mCherry-MAP1LC3B, and treated with DMSO or MG132. *A*=mitochondrial area normalised against total cell area (%). *n*=10 cells per condition from one representative experiment (of three). Data extend from min to max unless in (B), where they represent mean ± s.e.m. Scale bar: 10μm. **P* < 0.05, ***P* < 0.01, ****P* < 0.001 against the 'AURKA-GFP + DMSO' (A), the 'Empty vector + DMSO' (B,C), the 'AURKA-GFP' (D) or each corresponding 'AURKA-No acceptor' (E) conditions. NS: not significant.

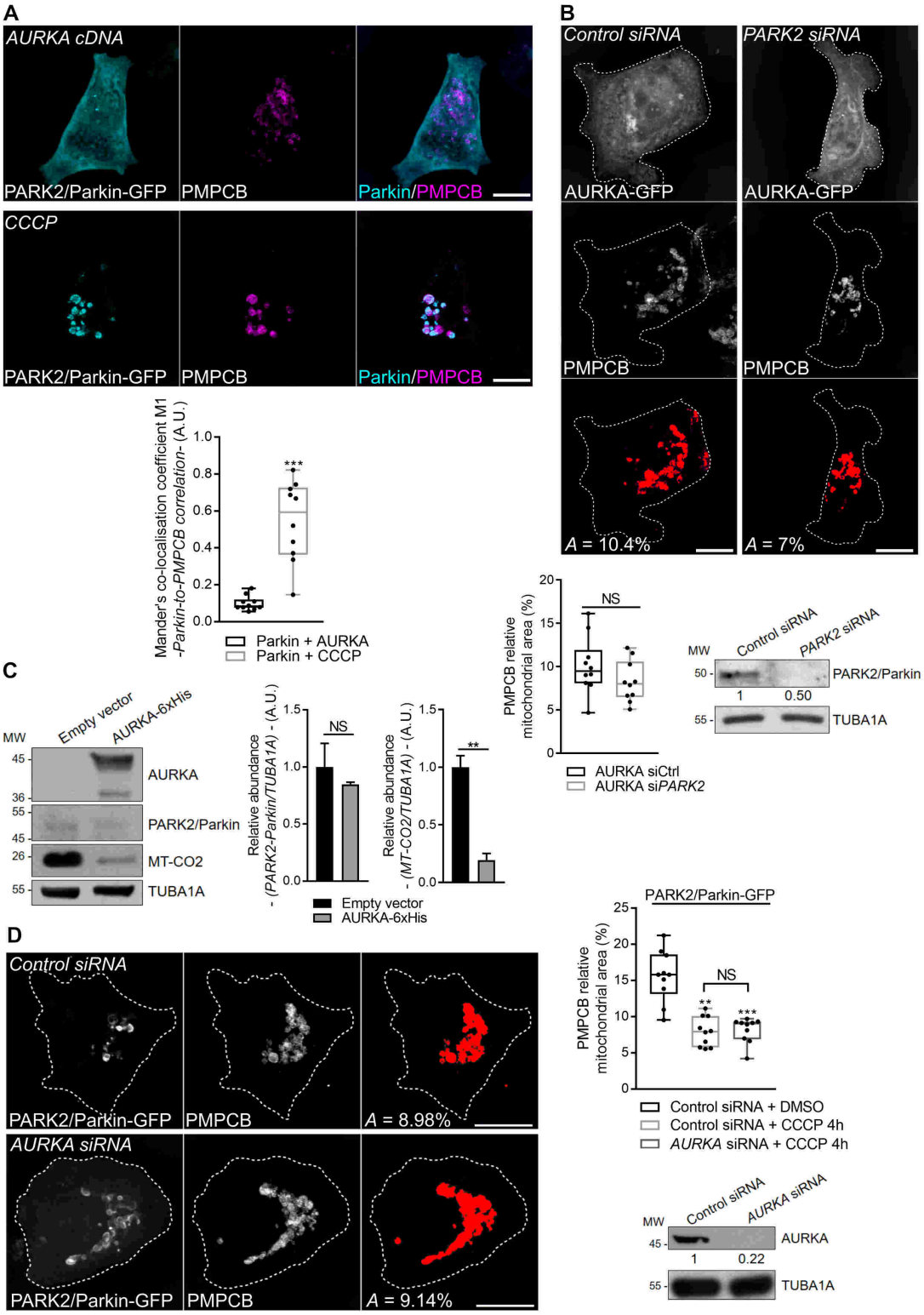

Fig. 4. AURKA induces mitophagy independently of PARK2/Parkin. Immunofluorescence micrographs of MCF7 cells co-expressing PARK2/Parkin-GFP and AURKA (left panels), or overexpressing PARK2/Parkin-GFP and treated with CCCP (right panels). Mitochondria were labelled with an anti-PMPCB antibody. PARK2/Parkin-GFP was pseudocoloured cyan, PMPCB was pseudocoloured magenta. Graph: corresponding colocalisation analyses (Mander's coefficient) between PARK2/Parkin-GFP and PMPCB. *n*=10 cells per condition from one representative experiment (of three). (B-D) Loss of PMPCB staining (threshold mask and corresponding quantification) in MCF7 cells co-transfected with AURKA-GFP and a control- or a *PARK2*-specific siRNA (B), or co-transfected with PARK2/Parkin-GFP and a control- or a *AURKA*-specific siRNA and treated with 4h CCCP where indicated (D). *A*=mitochondrial area normalised against total cell area (%). *n*=10 cells per condition from one representative experiment (of three) The efficiency of the *PARK2*- and of the *AURKA*-specific siRNAs was validated by western blotting; the abundance of PARK2/Parkin or of AURKA was normalised to that of the loading control, which was arbitrarily fixed at 1, and reported below each blot. (C) Representative immunoblot and quantification of the normalised abundance of PARK2-Parkin and of MT-CO2 in total lysates of HEK293 cells transfected as indicated. *n*=3 independent experiments Data extend from min to max (A-B) or represent mean ± s.e.m (C). Scale bar: 10μm. Loading control: TUBA1A. $^{**}P < 0.01$, $^{***}P < 0.001$ against the 'Parkin + AURKA' (A), the 'AURKA + siCtrl' (B) or the 'Empty vector' (C) conditions. NS: not significant.

Mitophagy in AURKA-overexpressing cells is independent of PARK2/Parkin.

Given that cells overexpressing AURKA have a sequential proteolysis similar to that observed in PARK2/Parkin-dependent mitophagy (Chan et al., 2011; Yoshii et al., 2011), we evaluated whether AURKA induces mitochondrial mass loss within this pathway or outside of it. We first evaluated whether PARK2/Parkin is an AURKA interactor. Neither PARK2/Parkin nor its partner PINK1 were retrieved in the proteomics data constituting the interactome of AURKA at interphase in HEK293 cells (Bertolin et al., 2018). However, failure in detecting these interactions could potentially reflect dynamic interactions taking place only when mitophagy is activated, and not when AURKA regulates mitochondrial morphology or ATP production (Bertolin et al., 2018). As the recruitment of PARK2/Parkin to mitochondria is among the first events in the degradation programme orchestrated by PARK2/Parkin and PINK1 (Pickrell and Youle, 2015), we used this as a functional readout of mitophagy activation. In cells overexpressing AURKA, PARK2/Parkin-GFP remained largely cytosolic and no colocalisation was observed between PARK2/Parkin and the mitochondrial marker PMPCB (Fig. 4A, left panels). On the contrary, PARK2/Parkin was entirely mitochondrial in cells treated with the mitochondrial uncoupler CCCP (Fig. 4A, right panels) (Narendra et al., 2008). These results indicate that although there is a visible loss in mitochondrial mass, no initiation of PARK2/Parkin-dependent mitophagy occurs in cells overexpressing AURKA. To corroborate these results, we explored whether the loss of mitochondrial mass observed in cells overexpressing AURKA depends on the presence of PARK2/Parkin. siRNA- mediated downregulation of *PARK2* in MCF7 cells overexpressing AURKA did not rescue mitochondrial elimination (Fig. 4B). As recently done for STX17-dependent mitophagy, which was shown to be independent of PARK2/Parkin (Xian et al., 2019), we found that PARK2/Parkin was not expressed when the overexpression of AURKA induced mitochondrial clearance, although we observed the concomitant loss of the IMM marker MT-CO2 (Fig. 4C). We also tested whether the absence of AURKA could alter PARK2/Parkin-dependent mitophagy in cells where PARK2/Parkin is overexpressed and mitochondria are depolarised with CCCP (Narendra et al., 2008). AURKA knockdown does not perturb the mitochondrial mass loss induced by CCCP-mediated depolarization in cells overexpressing PARK2/Parkin (Fig. 4D).

These results indicate that AURKA induces organelle clearance in a PARK2/Parkin-independent fashion, and that the two clearance pathways are independent.

AURKA interacts with PHB2 during mitophagy.

PHB2 is an integral component of the IMM, and together with the highly homologous protein PHB it forms the Prohibitin heterodimeric complex (Merkwirth et al., 2008). We previously identified the Prohibitin complex (PHB/ PHB2) as one of the most prominent interactors of AURKA at mitochondria by quantitative proteomics (Bertolin et al., 2018). This interaction was confirmed by FRET/FLIM analyses in MFC7 cells, where we observed significant AURKA-GFP ΔLifetime variations in zones where PHB-mCherry or PHB2-mCherry were present (Fig. 5A). Given the key role of PHB2, but not of PHB, in mitochondrial turnover (Wei et al., 2017), we focused on the interaction between AURKA and PHB2. The depletion of *PARK2* by siRNA-mediated gene downregulation did not abolish the interaction between AURKA and PHB2, further confirming that AURKA-dependent mitochondrial loss is independent of PARK2/Parkin (Fig. 5B, Supplementary Fig. 4A). We then examined whether the interaction between AURKA and PHB2 is due to the import of AURKA into mitochondria (Bertolin et al., 2018), or to a physical proximity between the two proteins after OMM rupture (Fig. 3C). To discriminate between these two possibilities, we first tested the interaction between the non-importable AURKA ΔNter with PHB2 by FRET/FLIM. With this construct, we observed that the AURKA/PHB2 proximity is abolished (Fig. 5C). Then, we analysed the capacity of AURKA to interact with PHB2 in the presence of MG132, which blocks OMM rupture when AURKA is overexpressed. In this case, FRET/FLIM analyses indicated that the physical interaction between AURKA and PHB2 is maintained (Supplementary Fig. 4C). These results show that OMM rupture events are not necessary for AURKA and PHB2 to interact, while the import of the kinase into mitochondria is required for its interaction with the mitophagy receptor.

We then verified the functional consequences of this interaction, by exploring whether overexpressed AURKA induced mitochondrial mass loss in a PHB2-dependent manner. We knocked-down *PHB2* by siRNA-mediated gene downregulation, and we quantified the loss of the mitochondrial marker PMPCB upon the overexpression of AURKA (Fig. 5D). In cells overexpressing AURKA and transfected with a control siRNA or a siRNA against *PHB*, the abundance of PMPCB was 50% less than in cells without exogenous AURKA. On the contrary, the loss of PMPCB was significantly mitigated in cells overexpressing AURKA and depleted of *PHB2*, indicating that PHB2 is essential for AURKA-dependent mitophagy.

Together, these results show that AURKA interacts with PHB2, and that this interaction is mandatory to trigger mitochondrial elimination.

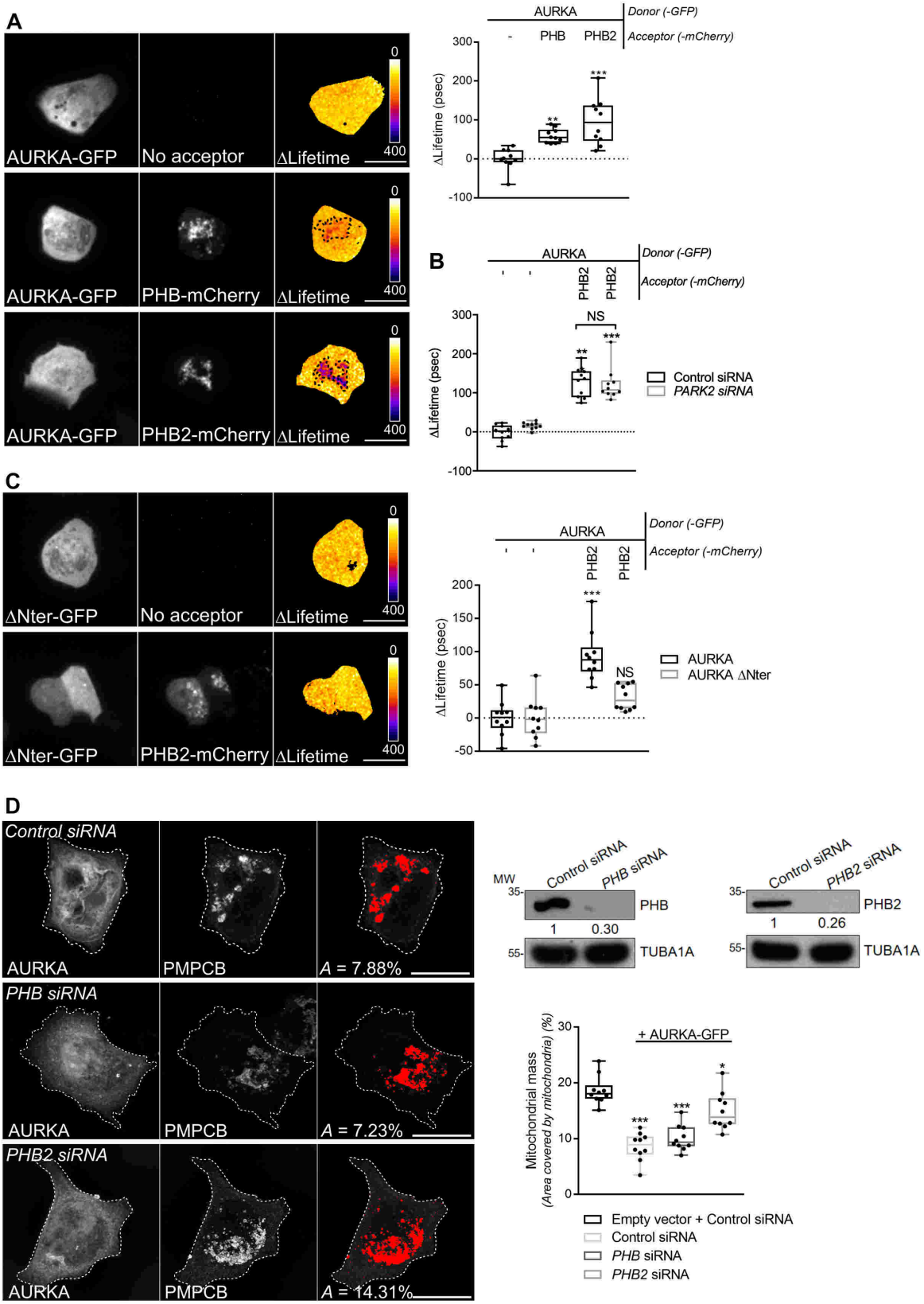

Fig. 5. The interaction of AURKA with PHB2 is mandatory for mitophagy. (A-C) FRET by FLIM analyses on MCF7 cells expressing AURKA-GFP alone or together with PHB-mCherry or PHB2-mCherry (A), co-expressing AURKA-GFP alone or together with PHB2-mCherry in the presence of a control- or a *PARK2*-specific siRNA (B), or expressing AURKA ΔNter-GFP alone or together with PHB2-mCherry. (C) Pseudocolour scale: pixel-by-pixel ΔLifetime. Dots: mitochondria-rich area. (D) Loss of PMPCB staining (threshold mask and corresponding quantification) in MCF7 cells co-transfected with an empty vector or with AURKA-GFP and a control-, a *PHB*- or a *PHB2*-specific siRNA as indicated. *A*=mitochondrial area normalised against total cell area (%). *n*=10 cells per condition from one representative experiment (of three). The efficiency of the *PHB*- and of the *PHB2*-specific siRNAs was validated by western blotting; the abundance of PHB or of PHB2 was normalised to that of the loading control, which was arbitrarily fixed at 1, and reported below each blot. Loading control: TUBA1A. Data extend from min to max. Scale bar: 10μm. **P* < 0.05, ***P* < 0.01, ****P* < 0.001 against the 'AURKA-no acceptor' (A, B), or the 'Empty vector + Control siRNA' (C) conditions. NS: not significant.

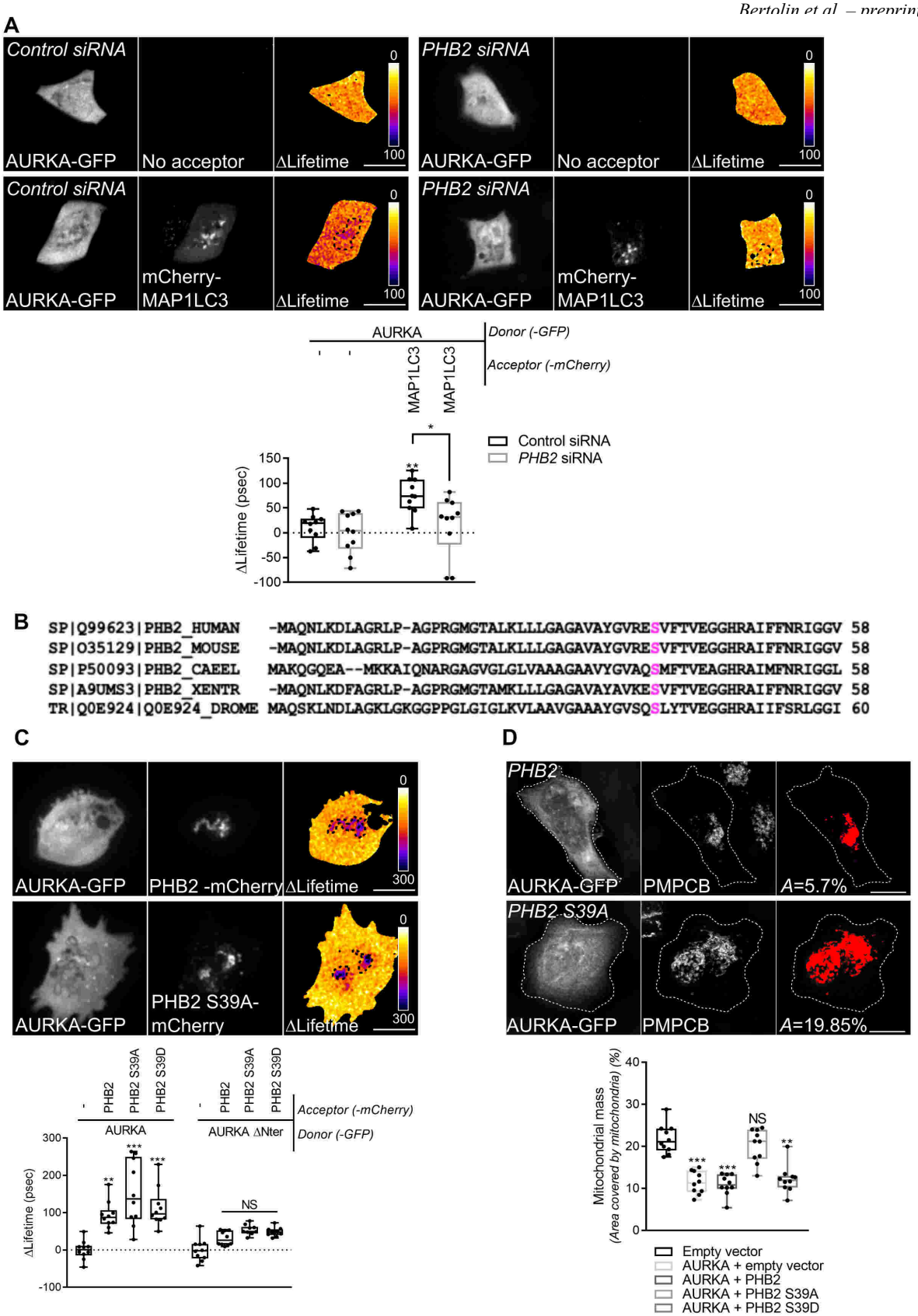

Fig. 6. The phosphorylation of PHB2 on Ser39 is mandatory for mitophagy. (A) FRET by FLIM analyses on MCF7 cells expressing AURKA-GFP alone or together with mCherry-MAP1LC3B in the presence of a control- or a *PHB2*-specific siRNA. Dotted area: autophagosome/autolysosome-rich areas. Pseudocolour scale: pixel-by-pixel ΔLifetime. Graph: corresponding ΔLifetime quantifications in the dotted area. *n*=10 cells per condition of one representative experiment (of three). (B) Clustal-Omega multi-species alignment of the PHB2 region comprising Ser39. Ser39 is indicated in magenta. Uniprot accession numbers used for the alignment are indicated. (C) Representative images and FRET by FLIM analyses on MCF7 cells expressing AURKA-GFP or AURKA ΔNter-GFP alone, or together with normal PHB2, PHB2 S39A or PHB2 S39D-mCherry. Graph: corresponding ΔLifetime quantifications in the dotted area.Dots: mitochondria-rich area. Pseudocolour scale: pixel-by-pixel ΔLifetime. (D) Loss of PMPCB staining (threshold mask and corresponding quantification) in MCF7 cells co-transfected with an empty vector or with AURKA-GFP and PHB2- 6xHis, PHB2 S39A-6xHis or PHB2 S39D-6xHis as indicated. *A*=mitochondrial area normalised against total cell area (%). *n*=10 cells per condition from one representative experiment (of three). Data extend from min to max. Scale bar: 10μm. **P* < 0.05, ***P* < 0.01, ****P* < 0.001 against the 'AURKA-no acceptor' (A, C), or the 'Empty vector' (D) conditions. NS: not significant.

AURKA triggers mitophagy via the phosphorylation of PHB2 on Ser39.

Given that AURKA interacts both with PHB2 and with MAP1LC3 in the context of mitochondrial elimination, we hypothesised that the interaction between AURKA and MAP1LC3 at mitochondria was mediated by PHB2. FRET/FLIM analyses performed in *PHB2*-depleted cells revealed that AURKA and MAP1LC3 no longer interacted in the absence of the mitophagy receptor (Fig. 6A). As the presence of PHB2 is mandatory to achieve mitochondrial elimination when AURKA is overexpressed, we explored whether PHB2 could be a substrate of AURKA. *In silico* simulations of AURKA-dependent phosphorylation using the GPS (Xue et al., 2005) or the PhosphoPICK (Patrick et al., 2016) methods, identified Ser39 as the only residue potentially phosphorylatable by AURKA which is conserved throughout evolution (Fig. 6B). We therefore evaluated whether a mutant of PHB2 that cannot be phosphorylated on Ser39 retained its capacity to interact with AURKA. To this end, we mutated Ser39 into Ala and we analysed the capacity of this construct to interact with the kinase by FRET/FLIM analyses. AURKA still interacted with PHB2 when Ser39 was converted into an Ala, indicating that the phosphorylation of this residue is not necessary for AURKA and PHB2 to interact (Fig. 6C and Supplementary Fig. 5A). As shown above for non-mutated PHB2 (Fig 5A), the interactions between AURKA and PHB2 S39A or the phospho-mimetic S39D were abolished with the non-importable AURKA ΔNter (Fig. 6C and Supplementary Fig. 5B).

Although the phosphorylation of this residue seems not to be required for AURKA to directly interact with PHB2, its conservation throughout evolution led us to hypothesise that it could still play a role in AURKA-dependent mitophagy. Therefore, we analysed the loss of PMPCB in cell overexpressing AURKA and PHB2, its S39A or S39D counterparts by confocal microscopy. We observed that the expression of PHB2 S39A abolished AURKA-dependent mitochondrial loss, while its phospho-mimicking mutant restored it (Fig. 6D and Supplementary Fig. 5C).

Our results show that AURKA and MAP1LC3 interaction depends on PHB2, and that the phosphorylation of Ser39 is required for mitophagy when the kinase is overexpressed.

The phosphorylation of PHB2 on Ser39 is mandatory to create a functional AURKA-MAP1LC3-PHB2 tripartite complex

A PHB2 S39A phosphor-inactive mutant impairs mitophagy without perturbing the AURKA/PHB2 protein-protein interaction. We then analysed whether PHB2 Ser39 phosphorylation was necessary for AURKA to interact with MAP1LC3. Again, we employed FRET/FLIM analyses to sense the interaction between AURKA and MAP1LC3 in the presence of PHB2, PHB2 S39A and PHB2 S39D. No difference was observed in the capacity of AURKA to interact with MAP1LC3, regardless of the PHB2 variant employed (Fig. 7A). The overexpression of PHB2 was recently shown to induce mitophagy *per se* within the PINK1/PARK2-Parkin pathway (Yan et al., 2019). Given that AURKA interacts with MAP1LC3 regardless of the PHB2 variant used, we sought to verify whether we were triggering an additional mitophagy pathway by simply overexpressing PHB2. In this light, we used the lipidation rate of MAP1LC3 as a marker of mitophagy initiation in the presence of GFP-tagged PHB2, PHB2 S39A and S39D and in the absence of overexpressed AURKA. The overexpression of PHB2 or its variants did not induce alterations in the lipidation rate of MAP1LC3 compared to control cells, nor on the abundance of endogenous PHB2 (Fig. 7B). Therefore, the overexpression of PHB2, PHB2 S39A or PHB2 S39D do not trigger mitophagy activation under these conditions. This also reinforces the central role of overexpressed AURKA as a main activator of mitophagy and mitochondrial mass loss.

Recent evidence showed that PHB2 acts as the receptor of lipidated, active MAP1LC3 on the IMM during mitophagy (Wei et al., 2017). Accordingly, we explored whether we could retrieve a PHB2/MAP1LC3 interaction by FRET/FLIM. The positive ΔLifetime between PHB2-GFP and mCherry-MAP1LC3B in cells overexpressing AURKA confirmed the existence of a tripartite complex constituted by these proteins (Fig. 7C). We then assessed whether the phosphorylation of PHB2 on Ser39 was necessary for PHB2 and MAP1LC3 to interact. FRET/FLIM analyses revealed that the PHB2 S39A variant abolished the interaction between PHB2 and MAP1LC3, which was restored in the presence of the corresponding phospho-mimetic version, PHB2 S39D (Fig. 7C).

These results indicate the existence of a tripartite complex where AURKA, PHB2 and MAP1LC3 interact. The phosphorylation of PHB2 on Ser39 is mandatory to build a functional tripartite complex, as PHB2 is incapable to perform FRET with MAP1LC3 if Ser39 is not phosphorylated. Failure in building a functional tripartite complex – by altering one of the protein-protein proximities within the complex – abolishes mitophagy (Fig. 6D).

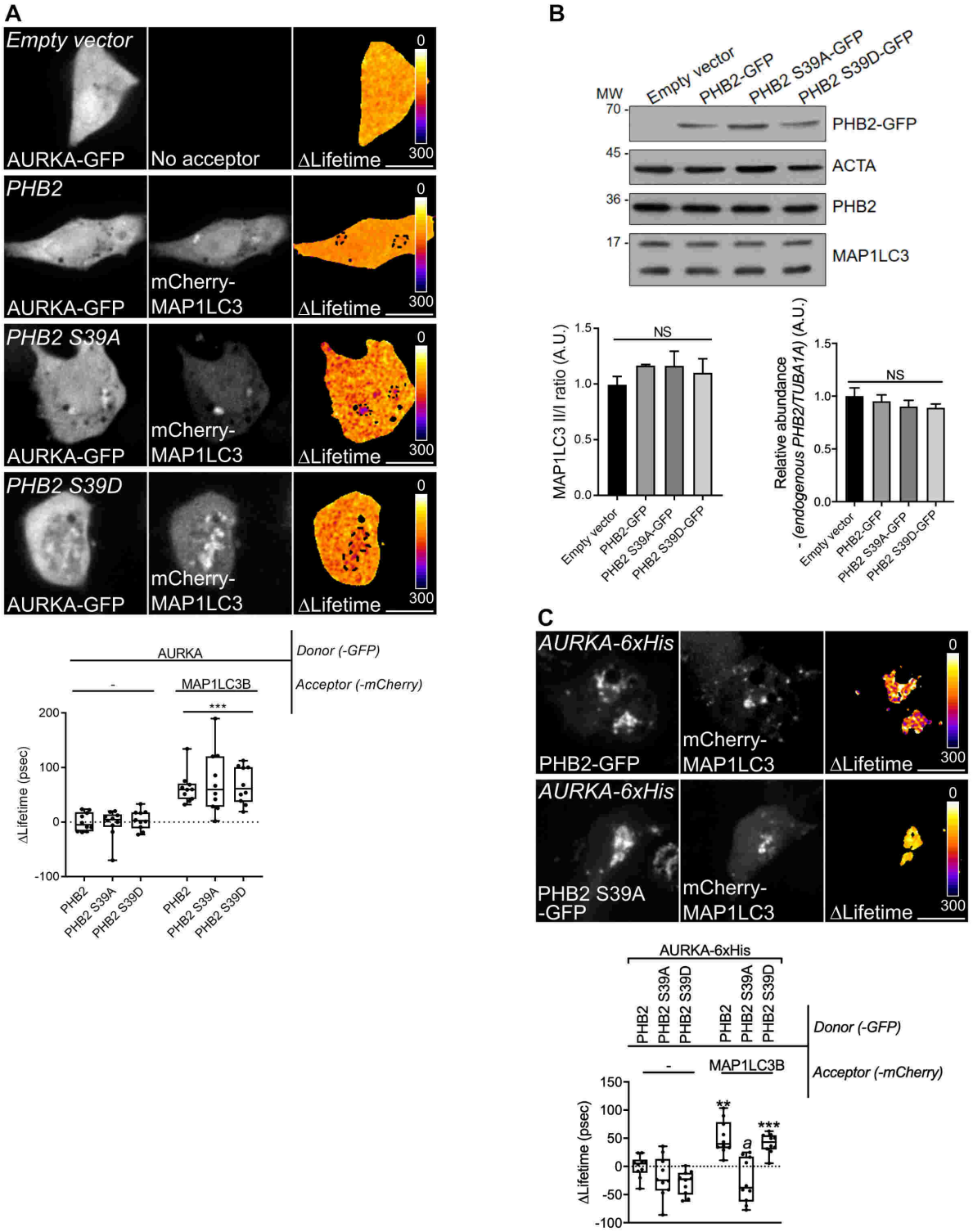

Fig. 7. AURKA forms a tripartite complex with PHB2 and MAP1LC3 upon the induction of mitophagy. (A) FRET by FLIM analyses on MCF7 cells expressing AURKA-GFP alone or together with mCherry-MAP1LC3B, and in the presence of the indicated PHB2-6xHis variants. Dotted area: autophagosome/autolysosome-rich areas. Graph: corresponding ΔLifetime quantifications in the dotted area. *n*=10 cells per condition of one representative experiment (of three). (B) Representative immunoblot and quantification of the MAP1LC3II/I ratio and of the normalised abundance of endogenous PHB2 in total lysates of HEK293 cells transfected as indicated. Loading control: ACTA. *n*=3 independent experiments. (C) FRET by FLIM analyses on MCF7 cells co-expressing AURKA-6xHis and PHB2-GFP or its S39A and S39D variants, alone or together with mCherry-MAP1LC3B. Graph: corresponding ΔLifetime quantifications. *n*=10 cells per condition of one representative experiment (of three). Pseudocolour scale: pixel-by-pixel ΔLifetime. Scale bar: 10μm. Data represent means ± s.e.m, unless in (A, C) where they extend from min to max. ***P*<0.01, ****P*<0.001 compared to each corresponding 'No acceptor' (A, C) conditions in cells transfected with AURKA and PHB2. [a]*P*<0.001 compared to the 'PHB2-MAP1LC3' or the 'PHB2 S39A-MAP1LC3' conditions. NS: not significant. A.U.: arbitrary units.

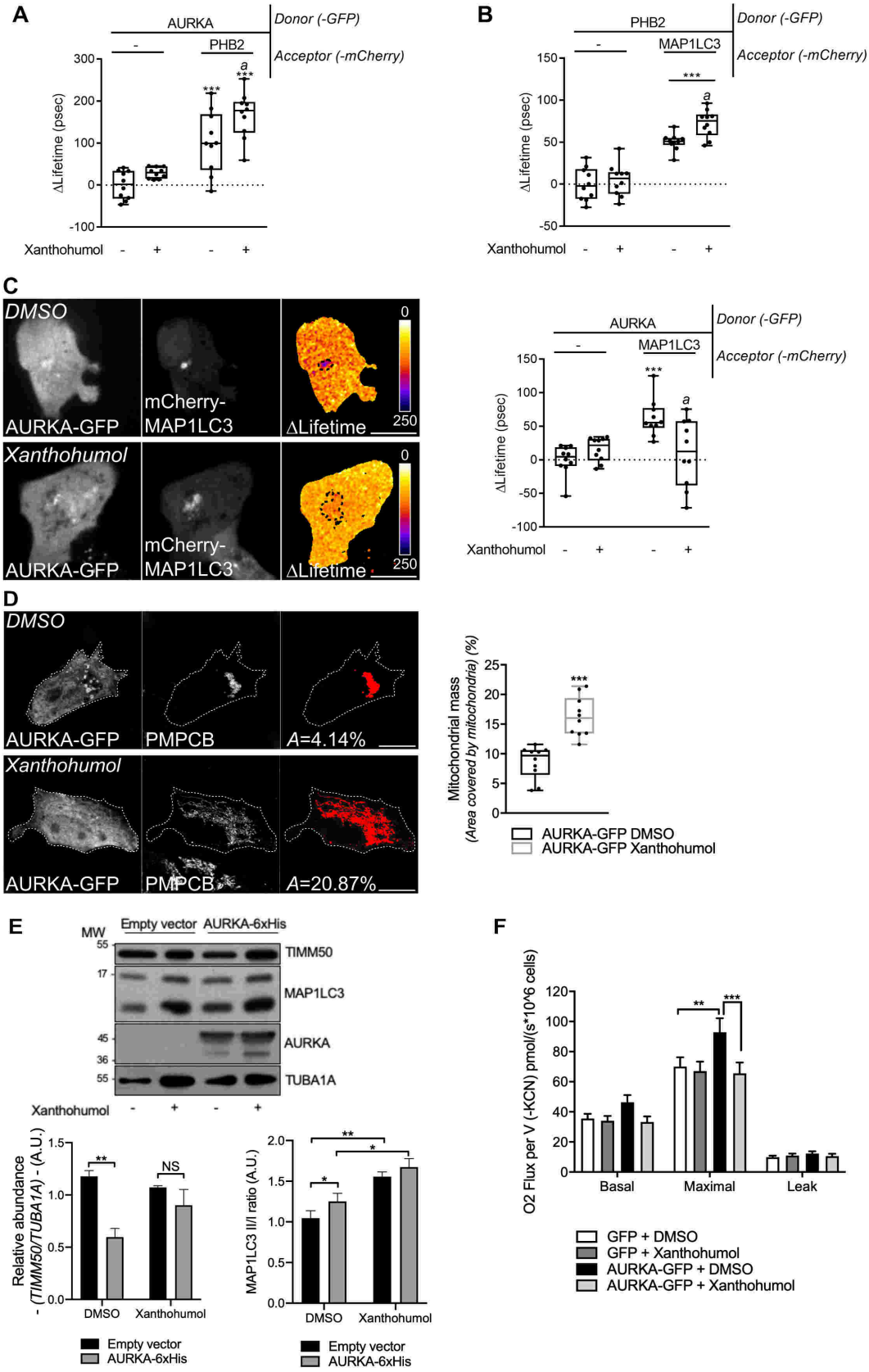

Fig. 8. Treatment with Xanthohumol blocks the interaction of AURKA with MAP1LC3, impairs mitophagy and blocks AURKA-dependent ATP increase. (A-C) FRET by FLIM analyses on MCF7 cells expressing AURKA-GFP alone or together with PHB2-mCherry (A), PHB2-GFP alone or together with mCherry-MAP1LC3B (B), or AURKA-GFP alone or together with mCherry-MAP1LC3B (C) and treated with DMSO or with Xanthohumol for 24h. Dotted area: autophagosome/autolysosome-rich areas. *n*=10 cells per condition of one representative experiment (of three). (D) Loss of PMPCB staining (threshold mask and corresponding quantification) in MCF7 cells co-transfected with AURKA-GFP and treated as indicated. *A*=mitochondrial area normalised against total cell area (%). *n*=10 cells per condition from one representative experiment (of three). (E) Representative immunoblot and quantification of the normalised abundance of TIMM50 and the MAP1LC3II/I ratio in total lysates of HEK293 cells transfected as indicated and treated with DMSO or Xanthohumol for 24h. Loading control: TUBA1A. *n*=3 independent experiments. (F) Mitochondrial respiration of HEK293 cells overexpressing GFP or AURKA-GFP and treated with DMSO or Xanthohumol. *n*=3 independent experiments. Pseudocolour scale: pixel-by-pixel ΔLifetime. Scale bar: 10µm. Data extend from the 10th to the 90th percentile unless in (E), where they represent means ± s.e.m. **P* < 0.05, ***P* < 0.01, ****P*<0.001 compared to each corresponding 'No acceptor' (A-C), 'AURKA-GFP DMSO' (D), 'DMSO' (E), or 'GFP + DMSO' or 'AURKA-GFP + DMSO' (F) conditions. *a*= ***P* < 0.01 compared to each corresponding '-' condition (A-C) NS: not significant. A.U.: arbitrary units.

The PHB2 ligand Xanthohumol inhibits mitophagy by impairing the tripartite complex, and it abolishes the AURKA-dependent ATP overproduction

In the attempt of blocking AURKA-dependent mitophagy, we next looked for a pharmacological strategy to block the formation of a functional tripartite AURKA-MAP1LC3-PHB2 complex. The PHB2 ligand Xanthohumol is a particularly interesting molecule in this context. It is a natural derivative of hop, which can block PHB2 functions in the nucleus (Yoshimaru et al., 2015). It can also block autophagy by targeting Valosin-Containing Protein (VCP) and impairing the autophagosome-lysosome fusion (Sasazawa et al., 2012).

We first analysed whether a functional tripartite AURKA-MAP1LC3-PHB2 complex was maintained upon treatment with Xanthohumol. The incubation of cells with Xanthohumol for 24h did not abolish the interaction between AURKA and PHB2 (Fig. 8A), nor the one between PHB2 and MAP1LC3B (Fig. 8B). Of note, these interactions were significantly reinforced after Xanthohumol treatment. Instead, FRET/FLIM analyses revealed that Xanthohumol alters the proximity between AURKA and MAP1LC3B (Fig. 8C). We previously observed that a dephosphorylated Ser39 in PHB2 destabilises protein-protein interactions within the tripartite complex (Fig. 7C), and that a destabilised AURKA-MAP1LC3 interaction results in an impaired mitophagy (Fig. 6A). We thus reasoned that the Xanthohumol-mediated perturbation of protein-protein proximities within the functional tripartite complex could also be indicative of defective mitophagy. Therefore, we explored whether mitochondrial mass loss could be rescued in cells over-expressing AURKA and treated with this compound. As expected, we quantified a significant loss of PMPCB staining when cells overexpressing AURKA were treated with DMSO (Fig. 8D). On the contrary, cells treated with Xanthohumol showed an increase in PMPCB staining (Fig. 8D), indicative of an increase in mitochondrial mass similar to that observed in cells not overexpressing AURKA (Fig. 1A). This observation was corroborated with western-blotting analyses illustrating the increase of the IMM marker TIMM50 after treating cells with Xanthohumol (Fig. 8E). By using the MAP1LC3II/I ratio to monitor the autophagic flux, we detected an increased MAP1LC3II accumulation and MAP1LC3II/I ratio in cells treated with this compound (Fig. 8E). These two parameters indicate that the autophagic flux is stalled, similarly to previous reports (Sasazawa et al., 2012).

Last, we asked whether treatment with Xanthohumol would revert the increased ATP production induced by AURKA overexpression (Bertolin et al., 2018). Therefore, we performed oxygen consumption rate (OCR) experiments, which measure the mitochondrial respiration capacity. As previously reported (Bertolin et al., 2018), cells overexpressing AURKA-GFP show an increased maximal respiration compared to cells expressing GFP alone (Fig. 8F). This effect was abolished when cells overexpressing AURKA were treated with Xanthohumol, while no effect of this compound was observed in control cells expressing GFP (Fig. 8F).

In conclusion, we here show that AURKA forms a mitophagy-inducing tripartite complex with PHB2 and MAP1LC3 (Fig. 9, left), upon the phosphorylation of PHB2 on Ser39. In addition, we show at AURKA-dependent mitophagy does not rely on the PARK2-Parkin/PINK1 pathway. Last, abolishing protein-protein proximities within the tripartite complex creates a “dysfunctional” tripartite complex and blocks AURKA-dependent mitochondrial clearance, as observed with a Ser39A phospho-inactive mutant. Alternatively, the natural PHB2 ligand Xanthohumol provides a pharmacological strategy to block the formation of a functional tripartite complex by altering the proximity between AURKA and MAP1LC3 (Fig. 9, right). This ultimately rescues AURKA-dependent mitochondrial loss, and it abolishes the excessive ATP production detected under AURKA overexpression. Therefore, this corroborates the existence of a metabolic switch upon the overexpression of AURKA, and it further reinforces the link between the efficiency of mitophagy and the metabolic capacity of cancer cells.

Discussion

We here show that the multifunctional kinase AURKA plays a previously uncovered role at mitochondria, where it is a key actor of organelle clearance by mitophagy. This novel role further broadens our understanding of the molecular functions of AURKA at mitochondria (Bertolin et al., 2018; Grant et al., 2018; Kashatus et al., 2011).

The largest body of evidence concerning the pathways of mitophagy focuses on the PINK1/PARK2-Parkin molecular axis (Pickrell and Youle, 2015). After nearly two decades of studies, there is general consensus that mitophagy pathways independent of PINK1/PARK2-Parkin exist, and that they play significant roles in specific pathological conditions as cancer, cardiac ischemia and neurodegenerative disorders (reviewed in (Villa et al., 2018). We here report that AURKA induces organelle turnover by interacting with MAP1LC3 on the mitophagy receptor PHB2, and without the contribution of PARK2/Parkin. Interestingly, this is the first evidence for a role of PHB2 outside of the PINK1-PARK2/Parkin pathway, which further extends the importance of this IMM receptor for various mitophagy

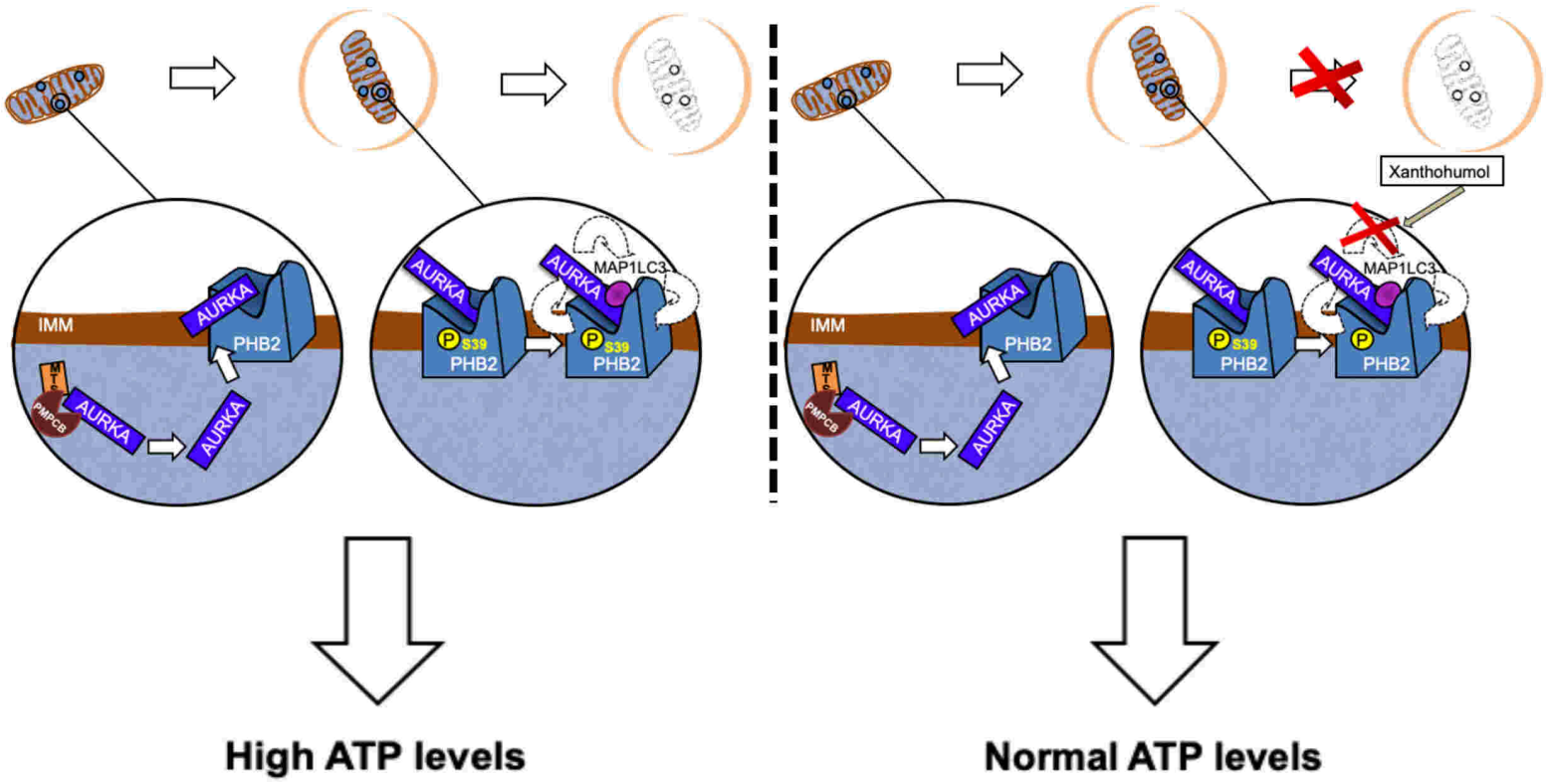

Fig. 9. Formation of the tripartite AURKA-PHB2-MAP1LC3 complex during AURKA-dependent mitophagy, and potential inhibition strategies with Xanthohumol. (Left panels) After being imported into mitochondria, AURKA interacts with the mitophagy receptor PHB2. The phosphorylation of Ser39 on PHB2 is mandatory for a functional AURKA-PHB2-MAP1LC3 complex to form, and to complete mitochondrial clearance in paradigms when AURKA is overexpressed. Under these conditions, mitochondrial ATP levels are high. Protein-protein interactions within the tripartite complex are illustrated with dashed arrows. (Right panels) A functional tripartite complex can be blocked by using the PHB2 ligand Xanthohumol. This compound alters AURKA-MAP1LC3 proximity, creating a dysfunctional tripartite complex. This results in impaired mitophagy and in restoration of normal ATP levels.

paradigms. The finding that AURKA-dependent mitochondrial clearance does not require PARK2/Parkin opens several perspectives for future studies. Although proteasome-dependent OMM rupture occurs in AURKA-overexpressing cells, it remains to be determined what E3 ubiquitin-protein ligase(s) can trigger this event. It is known that AURKA itself is targeted to the Ubiquitin-Proteasome system through Lys48- and Lys11-linked ubiquitin chains (Min et al., 2015). This occurs at mitotic exit, where the E3 Ubiquitin ligase APC/C decreases the relative abundance of the kinase before a new cell cycle begins. Outside of mitosis and before cells re-enter the G2/M phase, other E3 ligases as CHFR (Yu et al., 2005) and the SCF complex members FBXW7, FBXL7, and FBXL2 (Chen et al., 2013; Coon et al., 2012; Fujii et al., 2006; Hagedorn et al., 2007) are thought to induce the turnover of AURKA. It has been proposed that only small subpopulations of AURKA are targeted to the proteasome from each of these E3 ligases (Lindon et al., 2016). Does a yet undiscovered mitochondrial E3 ubiquitin ligase trigger OMM rupture upon AURKA overexpression? Alternatively, is there a partner of AURKA on the OMM, which could serve as a platform regulating the rupture of this membrane in a kinase-dependent manner? Interestingly, the AURKA domain targeted for APC/C-mediated ubiquitylation and degradation – located between residues 31-66 (Castro et al., 2002; Littlepage and Ruderman, 2002) – partially contains the MTS of the kinase, and it is lost upon AURKA import into the mitochondrial matrix (Bertolin et al., 2018; Grant et al., 2018). In this light, it is tempting to speculate that the mitochondrial import of AURKA is a way of protecting the kinase from proteasome-targeted ubiquitylation, allowing AURKA to perform selective functions on the IMM. Future studies are mandatory to elucidate these first steps in AURKA-dependent mitophagy, together with the definition of the other molecular players involved.

Given the breadth of the AURKA interactome, it is conceivable that the kinase plays different roles within the same subcellular compartment. However, a fascinating question – still unanswered – is whether one pool of AURKA (e.g. the mitochondrial one) is capable of triggering all the functions of the kinase at a given location, or whether sub-organellar pools of the

protein exist. To optimise anti-cancer therapies, it is essential to explore how the kinase orchestrates its functions in time and space within one single subcellular compartment. Structural biology data revealed that the interaction of AURKA with a substrate needs a two-step conformational change. Firstly, the kinase activates itself through the autophosphorylation on Thr288 (Bayliss et al., 2003; Cheetham, 2002; Walter et al., 2000; Zhang et al., 2007). This modification induces a "permissive" change in the conformation of the kinetic pocket, and increasing AURKA kinase activity in cells and in *Xenopus laevis* (Cheetham, 2002; Littlepage et al., 2002; Zhang et al., 2007). Secondly, the interaction with an activator as TPX2 further buries the phosphorylated Thr288 in the kinetic pocket of the kinase, and makes it inaccessible to phosphatases (Bayliss et al., 2003). This locks the kinase in a fully active conformation, capable of interacting with its substrates (Brunet et al., 2004; Eyers et al., 2003; Kufer et al., 2002). Although the activation and activity events are needed for AURKA to phosphorylate its multiple partners (Nikonova et al., 2013), it should be noted that these events were mainly reported for mitotic interactors of AURKA at the mitotic spindle. Non-mitotic roles of AURKA are constantly arising (Bertolin and Tramier, 2019; Korobeynikov et al., 2017; Tsunematsu et al., 2015); a still unanswered question is whether the activation/activity mechanisms during interphase and at specific subcellular locations are identical to the mitotic ones (Vaufrey et al., 2018). The majority of the current AURKA inhibitors are designed to block the activation of the kinase by behaving as ATP analogues with higher affinity for the kinetic pocket (Damodaran et al., 2017). The efficacy of the available ATP analogues in anti-cancer therapies is poor, and none of the existing ones passed phase III of clinical trials (Bavetsias and Linardopoulos, 2015). However, combinatorial approaches of AURKA inhibitors together with microtubule-stabilising drugs were shown to be beneficial to patients (Lin et al., 2012; Mazumdar et al., 2009; Sehdev et al., 2013). In addition, *in silico* (Kong et al., 2018) and high-content FRET/FLIM studies (Sizaire et al., 2020), which rely on AURKA conformational changes, represent exciting new strategies to identify novel AURKA inhibitors using the conformational changes of the kinase. In the context of the mitochondrial functions of AURKA, the future challenge will be to integrate ATP analogues with compounds targeting one specific conformation, one specific function of the kinase, and at a given subcellular location. That would selectively block only selected roles of AURKA, while leaving the others unaffected.

In the perspective of optimising combinatorial therapies in the future, it would be exciting to explore the effects of combining AURKA inhibitors and Xanthohumol *in vivo*. This study represents the first piece of evidence that a single pharmacological compound can block at least two mitochondrial functions regulated by AURKA. Our data reinforce the concept that mitophagy and ATP production are in a mutual crosstalk (Melser et al., 2013, 2015), and they strongly suggest that overexpressed AURKA selects dysfunctional mitochondria for elimination, while sparing the metabolically-efficient ones in a fused network (Bertolin et al., 2018). However, the selectivity of Xanthohumol towards AURKA-dependent mitophagy should further be investigated. We are currently incapable of separating the roles of Xanthohumol as a ligand of PHB2 (Yoshimaru et al., 2015) and as a VCP inhibitor in autophagy (Sasazawa et al., 2012). In the case of AURKA-dependent mitophagy, the addition of this compound does not alter the proximity of PHB2 with the other members of the tripartite complex, but rather the one of AURKA and MAP1LC3. This could be linked to the autophagy-blocking properties of Xanthohumol playing a more prominent role in this experimental paradigm. In addition, FRET/FLIM data indicate that constituting a functional tripartite complex - where all protein-protein interactions occur - is necessary for mitophagy. In this light, the effect of Xanthohumol and of the S39A variant could modify the structure of the tripartite complex, or even create two bi-partite sub-complexes. Overall, our data call for future studies to better understand how the tripartite complex is structurally organised, and how Xanthohumol interferes with its stability.

In conclusion, we here show that overexpressed AURKA localised at mitochondria induces the degradation of mitochondria by mitophagy. This is achieved through the formation of a tripartite complex with MAP1LC3 and its IMM receptor PHB2. We also propose that this molecular mechanism is of relevance to cancer, as the remaining organelles form a fused mitochondrial network and show an increased capacity to produce ATP. Maintaining a population of highly-competent mitochondria might represent a way to sustain the metabolic demands of the cancer cell, while eliminating the less efficient organelles. Finally, blocking mitophagy by pharmacological means translates in lowering ATP production rates, thereby paving the way to novel strategies in counteracting the effects of the overexpression of AURKA in epithelial cancers.

Materials and Methods

Expression vectors and molecular cloning

The list of plasmids used in this study is reported in Supplementary Table 1. DNA constructs were either generated

using the Gibson Assembly Master Mix (New England Biolabs), or the T4 DNA ligase (Thermo Fisher Scientific). Where indicated, plasmids were directly purchased from Addgene. Site-directed mutagenesis reactions were performed by Quick-Change site-directed mutagenesis (Stratagene). All cloning and mutagenesis reactions were verified on a 3130 XL sequencer (Applied Biosystems).

Cell culture procedures

MCF7 (HTB-22) and HEK293 (CRL-1573) cells were purchased from the American Type Culture Collection (ATCC) and were free from mycoplasma. They were grown in Dulbecco's modified Eagle's medium (DMEM, Thermo Fisher Scientific) supplemented with 10% foetal bovine serum (FBS, Thermo Fisher Scientific), 1% L-glutamine (Thermo Fisher Scientific) and 1% penicillin–streptomycin (Thermo Fisher Scientific). For all live microscopy experiments, cells were grown at 37°C in Nunc Lab-Tek II Chamber slides (Thermo Fisher Scientific). Standard growth media was replaced with phenol red-free Leibovitz's L-15 medium (Thermo Fisher Scientific) supplemented with 20% foetal bovine serum and 1% penicillin–streptomycin prior to imaging. AllStars negative control (SI03650318) and functionally-validated siRNAs against *PHB* (SI02223557) and *PHB2* (SI02780918) were purchased from Qiagen; the siRNA against *AURKA* was synthesised and purchased from Eurogentec, as previously described (Bertolin et al., 2016) (sequence: 5'-AUGCCCUGUCUUACUGUCA-3'). The *PARK2*-specific siRNA was purchased from Thermo Fisher Scientific (HSS107593). The *AURKA*-specific shRNA (SHCLNG-NM_003600) and a non-targeting control (SHC002) were purchased from Sigma-Aldrich. Plasmids shRNAs were transfected by the calcium phosphate method or with Lipofectamine 2000 (Thermo Fisher Scientific), according to the manufacturer's instructions. SiRNAs were transfected using Lipofectamine RNAiMAX (Thermo Fisher Scientific); co-transfections of plasmids and siRNAs were made with Lipofectamine 2000 according to the manufacturer's instructions. Cells were plated at 70% confluence in 24-well cell plates for immunocytochemistry, in 8-well or 4-well Nunc Lab-Tek II Chamber slides for live microscopy, or on 10 cm Petri dishes for total cell lysates or flow cytometry. Cells were harvested, fixed or imaged 48h after transfection. For flow cytometry, cells were rinsed twice in Ca^{2+}- and Mg^{2+}-free Phosphate Buffer Saline (Thermo Fisher Scientific), trypsinised (0.05% Trypsin – EDTA, Thermo Fisher Scientific) and resuspended in phenol-free L-15 medium.

Chemical reagents and fluorescent dyes

Carbonyl cyanide 3-chlorophenylhydrazone (Sigma-Aldrich, C2759) was used at a final concentration of 10µM for 4h before imaging. 3-Methyladenine (S2767, 5mM) and Bafilomycin A1 (S1413, 100 nM) were purchased from Selleck Chemicals and incubated for 24h prior to imaging or cell harvesting; MG-132 (S2619, 1µM) was purchased from Selleck Chemicals and incubated for 16h; Xanthohumol (S7889, 30µM (Sasazawa et al., 2012)) was purchased from Selleck Chemicals and incubated for 24h prior to imaging or cell harvesting for western blotting, or 6h prior to OCR measurements. All compounds were resuspended in Dimethylsulfoxide (DMSO, Euromedex, UD8050-A). Tetramethylrhodamine, methyl ester, perchlorate (TMRM, T668, Thermo Fisher Scientific, 50 nM) and MitoTracker Green FM (M7514, Thermo Fisher Scientific, 100nM) were simultaneously added to phenol-free L-15 medium and incubated for 30 min at 37°C prior to imaging or flow cytometry. Lysotracker Red DND-99 (Thermo Fisher Scientific) was used at a final concentration of 50 nM and incubated for 40 min at 37°C before flow cytometry.

Drosophila strains

Drosophila melanogaster stocks and crossings were set up and grown at 25°C. UAS-mito-HA-GFP (BDSC: 8443), UASp-mCherry-Atg8a (BDSC: 37750), UAS-aurA.Exel (BDSC: 8377) were obtained from the Bloomington Drosophila Stock Center. The scabrous-GAL4 (sca-GAL4) driver was obtained from (Mlodzik et al., 1990). $aurA^{ST}$ and $aurA^{2G}$ were used as in (Bertolin et al., 2018). w^{1118} pupae were used as wild-type controls for all experiments. All crossings and the corresponding abbreviations used in the paper are listed in Supplementary Table 3. Pupae were collected as white pupae, aged for 16 h at 25°C and mounted on glass slides prior to imaging. All images collected in this study were acquired from epithelial cells of the dorsal thorax (notum) at room temperature.

Western blotting procedures

Total protein fractions were obtained by lysing HEK cells in 50 mM Tris-HCl (pH 7.5), 150 mM NaCl, 1.5 mM MgCl2, 1% Triton X-100, and 0.5 mM dithiothreitol (DTT), supplemented with 0.2 mM Na3VO4, 4 mg/ml NaF, 5.4 mg/ml β-glycerophosphate and protease inhibitors (Complete Cocktail, Roche). Lysates were centrifuged at 13,000 g for 20 min at 4°C and frozen at -80°C for long-term storage. All protein fractions were quantified using the Bradford reagent (Bio-Rad). After resuspension in Laemmli sample buffer and boiling protein fractions were resolved by SDS–PAGE, transferred onto a nitrocellulose membrane (GE Healthcare) and analysed by western blotting. The list of primary antibodies and their working dilutions are provided in

Supplementary Table 2. The home-made anti-MT-CO2 antibody was provided by Dr. Anne Lombès (Cochin Institute, Paris, France) and published previously (Agier et al., 2012). Anti-mouse and anti-rabbit secondary antibodies conjugated to the horseradish-peroxidase (HRP) were purchased from Jackson ImmunoResearch Laboratories; anti-rat secondary antibodies conjugated to HRP were purchased from Bethyl Laboratories. The membranes were incubated with commercially available developing kit (Pierce), or a homemade enhanced chemiluminescence substrate made of 100 mM Tris (pH 8.6), 13 mg/ml coumaric acid (Sigma-Aldrich), 44 mg/ml luminol (Sigma-Aldrich) and 3% hydrogen peroxyde. Chemiluminescence signals were captured on film (Thermo Fisher Scientific), developed using a CURIX 60 developer (Agfa Healthcare) and quantified with Fiji software (NIH). The relative abundance of specific bands of interest was calculated by normalising the integrated density of each band towards the integrated density of loading controls.

Transmission electron microscopy

Cells were rinsed with 0.15 M sodium cacodylate and with 2.5% glutaraldehyde for 1 hr. After fixation, the cells were rinsed with 0.15 M sodium cacodylate and post-fixed with 1.5% osmium tetroxide for 1 hr. After further rinsing, the samples were dehydrated in increasing concentrations of ethanol (50, 70, 90% and 100% v/v). The cells were gradually infiltrated with increasing concentrations of epoxy resin (30, 50, 70% v/v in ethanol) for a minimum of 3 hr per concentration. The samples were then incubated overnight in pure epoxy resin before continuing with a two-step incubation in 2,4,6-Tris(dimethylaminomethyl)phenol (DMP30, Sigma-Aldrich)-epoxy resin, first for 3 hr and then for 24 hr at 60°C to polymerise the samples *en bloc*. Ultra-thin sections of 80 nm were cut from the blocks using a UC7 ultramicrotome (Leica), placed on grids, post-stained with uranyl acetate for 30 min and with lead citrate for 20 min. Sections were examined using a JEM-1400 Electron Microscope (JEOL Ltd.) operating at 120 kV accelerating voltage. Digital images were acquired using a Gatan SC1000 Orius® CCD camera with a dedicated imaging software (GataDigitalMicrographTM).

Immunocytochemistry, confocal and FLIM microscopy

Cells were fixed in 4% paraformaldehyde (Euromedex), stained using standard immunocytochemical procedures and mounted in ProLong Gold Antifade reagent (Thermo Fisher Scientific). The antibodies used were: primary monoclonal mouse anti-TOMM22 (Abcam, Ab10436); polyclonal rabbit anti-PMPCB, 1:500 (Proteintech, 16064–1-AP); and secondary anti-mouse or anti-rabbit antibodies conjugated to Alexa 674 at a 1:500 dilution, Alexa 555 or 488 both at a 1:5000 dilution (Thermo Fisher Scientific). Multicolour images of cultured cells were acquired with a Leica SP8 inverted confocal microscope (Leica) and a 63X oil-immersion objective (NA 1.4), a Leica SP5 inverted confocal microscope (Leica) and a 63X oil-immersion objective (NA 1.4) both driven by the Leica Acquisition Suite (LAS) software, or alternatively with a BX61WI FV-1000 confocal microscope (Olympus) driven by Olympus FV-1000 software and equipped with a 60X oil- immersion objective (NA 1.35). The excitation and emission wavelengths for GFP/MitoTracker Green were 488 and 525/50 nm, respectively; for TMRM/mCherry/Alexa 555, they were 561 and 605/70 nm; for Alexa 647 they were 633 and 650/20 nm. GFP was used as a FRET donor in all experiments, its decrease was measured by FLIM microscopy and the corresponding ΔLifetime was calculated as in (Bertolin et al., 2019). Fluorescence colocalisation was calculated with the JaCoP plugin (Bolte and Cordelieres, 2006) of the Fiji software after applying an automatic threshold mask to the confocal images. The same plugin was used to calculate TOMM22-negative/PMPCB-positive objects by normalising the objects with both mitochondrial markers on the total number of PMPCB-positive objects per image. This yielding values between 0 and 1, the PMPCB-only objects were calculated by subtracting each of the TOMM22-positive/PMPCB-positive values from 1. The relative mitochondrial area (A) was used to express mitochondrial mass, and it was calculated with Fiji software on maximal projections of confocal images acquired as above and following a previously-validated procedure (Bertolin et al., 2013). It was represented as the ratio between the area covered by the mitochondrial stain (TOMM22 or PMPCB), selected with an automatic threshold mask, and the total cell area.

Flow Cytometry

After incubation with MitoTracker Green FM or LysoTracker Red DND-99, cells were rinsed with PBS, trypsinised and centrifuged at 800g. Pellets were resuspended in sterile PBS, and the relative fluorescence intensity was measured with a FC500 flow cytometer (Beckman Coulter).

Oxygen consumption rate measurements

Before OCR measurements, cells were trypsinised and resuspended in normal growth medium. Measurements were carried out in the respiratory chamber of an Oroboros Oxygraph-2k (WGT). Cellular respiration was determined under basal conditions, with oligomycin (1 mg/ml, Sigma-Aldrich) to estimate leakage, and in the presence of increasing amounts (2.5–5 mM) of CCCP (Sigma-Aldrich) to calculate maximal

respiration. To inhibit mitochondrial respiration, 1 mM potassium cyanide was added (KCN, Sigma-Aldrich).

Statistical analyses

Two-way ANOVA tests were used to compare two variables among multiple conditions, one-way ANOVA tests was used to test one variable among multiple conditions, and Student's t-test or the Mann-Whitney test were employed to compare two conditions. All tests were performed after testing data for normality.

Two-way ANOVA and the Holm-Sidak method were used to compare the effect of the transfection conditions and of the status of the autophagy flux on the number of MAP1LC3 dots per cell (Supplementary Fig. 2B), the pharmacological treatment and the fluorescent proteins on ΔLifetime measurements (Fig. 3G; Fig. 8A-C; Supplementary Fig. 4B), the effect of the siRNA downregulation strategy and the fluorescent protein on ΔLifetime measurements (Fig. 5B-C; Fig. 6A-B), the effect of the the siRNA downregulation strategy and plasmid expression on the relative mitochondrial area (Fig. 5D), the effect of PHB2 isoforms and the fluorescent proteins on ΔLifetime measurements (Fig. 7A, D), the effect of the pharmacological treatment and the transfected vectors on the MAP1LC3 II/I cleavage ratio and on the abundance of mitochondrial markers (Fig. 8E), and the effect of the pharmacological treatment and the mitochondrial respiratory parameter on mitochondrial respiration (Fig. 8F).

One-way ANOVA and the Holm-Sidak method were used to compare mitochondrial mass calculated as the relative mitochondrial area (Fig. 1A), the MAP1LC3 II/I cleavage ratio (Fig 1B), the effect of the *Drosophila* genotype on the quantity of Atg8 at mitochondria (Supplementary Fig. 1A), the abundance of lysosomes in electron microscopy experiments (Fig. 2A), relative LysoTracker Red intensities (Fig. 2B), the red/green fluorescence ratio in cells transfected with mitoTandem (Supplementary Fig. 2A), pharmacological treatments on the relative mitochondrial area (Fig. 3A; Fig. 3C). One-way ANOVA on ranks and the Kruskal-Wallis method were used to compare relative MitoTracker Green intensities (Fig. 1C), the abundance of mitochondrial markers (Fig. 1F; Fig. 7B), the MAP1LC3 II/I cleavage ratio (Fig. 7B), ΔLifetime measurements with components of the autophagy pathway (Fig. 2C) or within the PHB complex (Fig. 5A), the relative mitochondrial area (Fig. 4D; Fig. 6D).

Student's t-test was used to compare the relative abundance of mitochondrial markers (Fig. 1B; Fig. 4B-C), the relative intensity of TMRM (Supplementary Fig. 1B) ΔLifetime measurements (Fig. 2D), pharmacological treatments on the relative mitochondrial area (Fig. 8D; Supplementary Fig. 3A-B), Mander's colocalisation coefficients (Fig. 3D; Fig. 4A). The Mann-Whitney test was used to compare Mander's colocalisation coefficients (Fig. 1C), the relative abundance of mitochondrial markers (Fig. 4C).

Acknowledgements

We thank A. Cheron for her invaluable technical help, and Drs. L. Buhlman and E. Baldini for critical reading and helpful discussions. We also thank Dr. A. Lombès for the generous gift of the anti-MT-CO2 primary antibody, and Dr. B. Levine for the gift of PHB and PHB2 cDNAs. We thank L. Deleurme of the flow cytometry and cell sorting platform (Biologie, Santé, Innovation Technologique, BIOSIT, Rennes, France), and we are grateful to S. Ley-Ngardigal and E.B. Gökerküçük for critical reading and technical assistance. We also thank S. Dutertre and X. Pinson from the Microscopy-Rennes Imaging Center (MRic, BIOSIT, Rennes, France) for advice, critical reading and constructive comments on image analysis. MRic is member of the national infrastructure France-BioImaging supported by the French National Research Agency (ANR-10-INBS-04). This work was supported by the *Centre National de la Recherche Scientifique*, the *Ligue Contre le Cancer Comités d'Ille et Vilaine, des Côtes d'Armor et du Finistère*, and the *Association pour la Recherche Contre le Cancer (ARC)* to G.B.

Author contributions

G.B. designed, performed and analysed the experiments, wrote the manuscript and provided funding. M.C A-G performed oxygen consumption rate experiments. A.B. performed electron microscopy. R. LB. provided support with the *Drosophila* model and help throughout the project. C.P. and M.T. reviewed the manuscript and provided support.

References

Agier, V., Oliviero, P., Lainé, J., L'Hermitte-Stead, C., Girard, S., Fillaut, S., Jardel, C., Bouillaud, F., Bulteau, A.L., and Lombès, A. (2012). Defective mitochondrial fusion, altered respiratory function, and distorted cristae structure in skin fibroblasts with heterozygous OPA1 mutations. Biochim. Biophys. Acta BBA - Mol. Basis Dis. *1822*, 1570–1580.

Andrésson, T., and Ruderman, J.V. (1998). The kinase Eg2 is a component of the Xenopus oocyte progesterone-activated

signaling pathway. EMBO J. *17*, 5627–5637.

Bavetsias, V., and Linardopoulos, S. (2015). Aurora Kinase Inhibitors: Current Status and Outlook. Front. Oncol. *5*.

Bayliss, R., Sardon, T., Vernos, I., and Conti, E. (2003). Structural basis of Aurora-A activation by TPX2 at the mitotic spindle. Mol. Cell *12*, 851–862.

Bertolin, G., and Tramier, M. (2019). Insights into the non-mitotic functions of Aurora kinase A: more than just cell division. Cell. Mol. Life Sci.

Bertolin, G., Ferrando-Miguel, R., Jacoupy, M., Traver, S., Grenier, K., Greene, A.W., Dauphin, A., Waharte, F., Bayot, A., Salamero, J., et al. (2013). The TOMM machinery is a molecular switch in PINK1 and PARK2/PARKIN-dependent mitochondrial clearance. Autophagy *9*, 1801–1817.

Bertolin, G., Sizaire, F., Herbomel, G., Reboutier, D., Prigent, C., and Tramier, M. (2016). A FRET biosensor reveals spatiotemporal activation and functions of aurora kinase A in living cells. Nat. Commun. *7*, 12674.

Bertolin, G., Bulteau, A.-L., Alves-Guerra, M.-C., Burel, A., Lavault, M.-T., Gavard, O., Le Bras, S., Gagné, J.-P., Poirier, G.G., Le Borgne, R., et al. (2018). Aurora kinase A localises to mitochondria to control organelle dynamics and energy production. ELife *7*.

Bertolin, G., Sizaire, F., Déméautis, C., Chapuis, C., Mérola, F., Erard, M., and Tramier, M. (2019). Optimized FRET Pairs and Quantification Approaches To Detect the Activation of Aurora Kinase A at Mitosis. ACS Sens. *4*, 2018–2027.

Bolte, S., and Cordelieres, F.P. (2006). A guided tour into subcellular colocalization analysis in light microscopy. J. Microsc. *224*, 213–232.

Brunet, S., Sardon, T., Zimmerman, T., Wittmann, T., Pepperkok, R., Karsenti, E., and Vernos, I. (2004). Characterization of the TPX2 Domains Involved in Microtubule Nucleation and Spindle Assembly in Xenopus Egg Extracts. Mol. Biol. Cell *15*, 5318–5328.

Castro, A., Vigneron, S., Bernis, C., Labbé, J.-C., Prigent, C., and Lorca, T. (2002). The D-Box-activating domain (DAD) is a new proteolysis signal that stimulates the silent D-Box sequence of Aurora-A. EMBO Rep. *3*, 1209–1214.

Chan, N.C., Salazar, A.M., Pham, A.H., Sweredoski, M.J., Kolawa, N.J., Graham, R.L.J., Hess, S., and Chan, D.C. (2011). Broad activation of the ubiquitin-proteasome system by Parkin is critical for mitophagy. Hum. Mol. Genet. *20*, 1726–1737.

Cheetham, G.M.T. (2002). Crystal Structure of Aurora-2, an Oncogenic Serine/Threonine Kinase. J. Biol. Chem. *277*, 42419–42422.

Chen, B.B., Glasser, J.R., Coon, T.A., and Mallampalli, R.K. (2013). Skp-cullin-F box E3 ligase component FBXL2 ubiquitinates Aurora B to inhibit tumorigenesis. Cell Death Dis. *4*, e759.

Coon, T.A., Glasser, J.R., Mallampalli, R.K., and Chen, B.B. (2012). Novel E3 ligase component FBXL7 ubiquitinates and degrades Aurora A, causing mitotic arrest. Cell Cycle Georget. Tex *11*, 721–729.

Damodaran, A.P., Vaufrey, L., Gavard, O., and Prigent, C. (2017). Aurora A Kinase Is a Priority Pharmaceutical Target for the Treatment of Cancers. Trends Pharmacol. Sci. *38*, 687–700.

Di Rita, A., Peschiaroli, A., D′Acunzo, P., Strobbe, D., Hu, Z., Gruber, J., Nygaard, M., Lambrughi, M., Melino, G., Papaleo, E., et al. (2018). HUWE1 E3 ligase promotes PINK1/PARKIN-independent mitophagy by regulating AMBRA1 activation via IKKα. Nat. Commun. *9*.

Eyers, P.A., Erikson, E., Chen, L.G., and Maller, J.L. (2003). A novel mechanism for activation of the protein kinase Aurora A. Curr. Biol. *13*, 691–697.

Farag, S.S. (2011). The potential role of Aurora kinase inhibitors in haematological malignancies: Review. Br. J. Haematol. *155*, 561–579.

Fujii, Y., Yada, M., Nishiyama, M., Kamura, T., Takahashi, H., Tsunematsu, R., Susaki, E., Nakagawa, T., Matsumoto, A., and Nakayama, K.I. (2006). Fbxw7 contributes to tumor suppression by targeting multiple proteins for ubiquitin-dependent degradation. Cancer Sci. *97*, 729–736.

Geisler, S., Holmström, K.M., Skujat, D., Fiesel, F.C., Rothfuss, O.C., Kahle, P.J., and Springer, W. (2010). PINK1/Parkin-mediated mitophagy is dependent on VDAC1 and p62/SQSTM1. Nat. Cell Biol. *12*, 119–131.

Giet, R., McLean, D., Descamps, S., Lee, M.J., Raff, J.W., Prigent, C., and Glover, D.M. (2002). Drosophila Aurora A kinase is required to localize D-TACC to centrosomes and to regulate astral microtubules. J. Cell Biol. *156*, 437–451.

Glover, D.M., Leibowitz, M.H., McLean, D.A., and Parry, H. (1995). Mutations in aurora prevent centrosome separation leading to the formation of monopolar spindles. Cell *81*, 95–105.

Grant, R., Abdelbaki, A., Bertoldi, A., Gavilan, M.P., Mansfeld, J., Glover, D.M., and Lindon, C. (2018). Constitutive regulation of mitochondrial morphology by Aurora A kinase depends on a

predicted cryptic targeting sequence at the N-terminus. Open Biol. *8*, 170272.

Hagedorn, M., Delugin, M., Abraldes, I., Allain, N., Belaud-Rotureau, M.-A., Turmo, M., Prigent, C., Loiseau, H., Bikfalvi, A., and Javerzat, S. (2007). FBXW7/hCDC4 controls glioma cell proliferation in vitro and is a prognostic marker for survival in glioblastoma patients. Cell Div. *2*, 9.

Hurley, J.H., and Young, L.N. (2017). Mechanisms of Autophagy Initiation. Annu. Rev. Biochem. *86*, 225–244.

Isakson, P., Lystad, A.H., Breen, K., Koster, G., Stenmark, H., and Simonsen, A. (2013). TRAF6 mediates ubiquitination of KIF23/MKLP1 and is required for midbody ring degradation by selective autophagy. Autophagy *9*, 1955–1964.

Kashatus, D.F., Lim, K.-H., Brady, D.C., Pershing, N.L.K., Cox, A.D., and Counter, C.M. (2011). RALA and RALBP1 regulate mitochondrial fission at mitosis. Nat. Cell Biol. *13*, 1108–1115.

Kim, I., Rodriguez-Enriquez, S., and Lemasters, J.J. (2007). Selective degradation of mitochondria by mitophagy. Arch. Biochem. Biophys. *462*, 245–253.

Kinzel, D., Boldt, K., Davis, E.E., Burtscher, I., Trümbach, D., Diplas, B., Attié-Bitach, T., Wurst, W., Katsanis, N., Ueffing, M., et al. (2010). Pitchfork Regulates Primary Cilia Disassembly and Left-Right Asymmetry. Dev. Cell *19*, 66–77.

Klionsky, D.J., Abdelmohsen, K., Abe, A., Abedin, M.J., Abeliovich, H., Acevedo Arozena, A., Adachi, H., Adams, C.M., Adams, P.D., Adeli, K., et al. (2016). Guidelines for the use and interpretation of assays for monitoring autophagy (3rd edition). Autophagy *12*, 1–222.

Kong, Y., Bender, A., and Yan, A. (2018). Identification of Novel Aurora Kinase A (AURKA) Inhibitors via Hierarchical Ligand-Based Virtual Screening. J. Chem. Inf. Model. *58*, 36–47.

Korobeynikov, V., Deneka, A.Y., and Golemis, E.A. (2017). Mechanisms for nonmitotic activation of Aurora-A at cilia. Biochem. Soc. Trans. *45*, 37–49.

Kufer, T.A., Silljé, H.H.W., Körner, R., Gruss, O.J., Meraldi, P., and Nigg, E.A. (2002). Human TPX2 is required for targeting Aurora-A kinase to the spindle. J. Cell Biol. *158*, 617–623.

Lazarou, M., Sliter, D.A., Kane, L.A., Sarraf, S.A., Wang, C., Burman, J.L., Sideris, D.P., Fogel, A.I., and Youle, R.J. (2015). The ubiquitin kinase PINK1 recruits autophagy receptors to induce mitophagy. Nature *524*, 309–314.

Lee, C.-Y., Andersen, R.O., Cabernard, C., Manning, L., Tran, K.D., Lanskey, M.J., Bashirullah, A., and Doe, C.Q. (2006). Drosophila Aurora-A kinase inhibits neuroblast self-renewal by regulating aPKC/Numb cortical polarity and spindle orientation. Genes Dev. *20*, 3464–3474.

Lee, K.H., Johmura, Y., Yu, L.-R., Park, J.-E., Gao, Y., Bang, J.K., Zhou, M., Veenstra, T.D., Yeon Kim, B., and Lee, K.S. (2012). Identification of a novel Wnt5a-CK1ε-Dvl2-Plk1-mediated primary cilia disassembly pathway: Primary cilia disassembly by the Dvl2-Plk1 complex. EMBO J. *31*, 3104–3117.

Leray, A., Padilla-Parra, S., Roul, J., Héliot, L., and Tramier, M. (2013). Spatio-Temporal Quantification of FRET in living cells by fast time-domain FLIM: a comparative study of non-fitting methods [corrected]. PloS One *8*, e69335.

Lin, Y., Richards, F.M., Krippendorff, B.-F., Bramhall, J.L., Harrington, J.A., Bapiro, T.E., Robertson, A., Zheleva, D., and Jodrell, D.I. (2012). Paclitaxel and CYC3, an aurora kinase A inhibitor, synergise in pancreatic cancer cells but not bone marrow precursor cells. Br. J. Cancer *107*, 1692–1701.

Lindon, C., Grant, R., and Min, M. (2016). Ubiquitin-Mediated Degradation of Aurora Kinases. Front. Oncol. *5*.

Littlepage, L.E., and Ruderman, J.V. (2002). Identification of a new APC/C recognition domain, the A box, which is required for the Cdh1-dependent destruction of the kinase Aurora-A during mitotic exit. Genes Dev. *16*, 2274–2285.

Littlepage, L.E., Wu, H., Andresson, T., Deanehan, J.K., Amundadottir, L.T., and Ruderman, J.V. (2002). Identification of phosphorylated residues that affect the activity of the mitotic kinase Aurora-A. Proc. Natl. Acad. Sci. U. S. A. *99*, 15440–15445.

Mazumdar, A., Henderson, Y.C., El-Naggar, A.K., Sen, S., and Clayman, G.L. (2009). Aurora kinase A inhibition and paclitaxel as targeted combination therapy for head and neck squamous cell carcinoma. Head Neck *31*, 625–634.

Melser, S., Chatelain, E.H., Lavie, J., Mahfouf, W., Jose, C., Obre, E., Goorden, S., Priault, M., Elgersma, Y., Rezvani, H.R., et al. (2013). Rheb Regulates Mitophagy Induced by Mitochondrial Energetic Status. Cell Metab. *17*, 719–730.

Melser, S., Lavie, J., and Bénard, G. (2015). Mitochondrial degradation and energy metabolism. Biochim. Biophys. Acta BBA - Mol. Cell Res. *1853*, 2812–2821.

Mercer, T.J., Gubas, A., and Tooze, S.A. (2018). A molecular perspective of mammalian autophagosome biogenesis. J. Biol. Chem. *293*, 5386–5395.

Mergen, M., Engel, C., Muller, B., Follo, M., Schafer, T., Jung, M., and Walz, G. (2013). The nephronophthisis gene product

NPHP2/Inversin interacts with Aurora A and interferes with HDAC6-mediated cilia disassembly. Nephrol. Dial. Transplant. *28*, 2744–2753.

Merkwirth, C., Dargazanli, S., Tatsuta, T., Geimer, S., Löwer, B., Wunderlich, F.T., Kleist-Retzow, J.-C. von, Waisman, A., Westermann, B., and Langer, T. (2008). Prohibitins control cell proliferation and apoptosis by regulating OPA1-dependent cristae morphogenesis in mitochondria. Genes Dev. *22*, 476–488.

Min, M., Mevissen, T.E.T., De Luca, M., Komander, D., and Lindon, C. (2015). Efficient APC/C substrate degradation in cells undergoing mitotic exit depends on K11 ubiquitin linkages. Mol. Biol. Cell *26*, 4325–4332.

Mishra, P., and Chan, D.C. (2016). Metabolic regulation of mitochondrial dynamics. J. Cell Biol. *212*, 379–387.

Mlodzik, M., Baker, N.E., and Rubin, G.M. (1990). Isolation and expression of scabrous, a gene regulating neurogenesis in Drosophila. Genes Dev. *4*, 1848–1861.

Mortensen, M., Ferguson, D.J.P., Edelmann, M., Kessler, B., Morten, K.J., Komatsu, M., and Simon, A.K. (2010). Loss of autophagy in erythroid cells leads to defective removal of mitochondria and severe anemia in vivo. Proc. Natl. Acad. Sci. *107*, 832–837.

Nakatogawa, H. (2013). Two ubiquitin-like conjugation systems that mediate membrane formation during autophagy. Essays Biochem. *55*, 39–50.

Narendra, D., Tanaka, A., Suen, D.-F., and Youle, R.J. (2008). Parkin is recruited selectively to impaired mitochondria and promotes their autophagy. J. Cell Biol. *183*, 795–803.

Nikonova, A.S., Astsaturov, I., Serebriiskii, I.G., Dunbrack, R.L., and Golemis, E.A. (2013). Aurora A kinase (AURKA) in normal and pathological cell division. Cell. Mol. Life Sci. *70*, 661–687.

Novak, I., Kirkin, V., McEwan, D.G., Zhang, J., Wild, P., Rozenknop, A., Rogov, V., Löhr, F., Popovic, D., Occhipinti, A., et al. (2010). Nix is a selective autophagy receptor for mitochondrial clearance. EMBO Rep. *11*, 45–51.

Padilla-Parra, S., Audugé, N., Coppey-Moisan, M., and Tramier, M. (2008). Quantitative FRET analysis by fast acquisition time domain FLIM at high spatial resolution in living cells. Biophys. J. *95*, 2976–2988.

Paris, J., and Philippe, M. (1990). Poly(A) metabolism and polysomal recruitment of maternal mRNAs during early Xenopus development. Dev. Biol. *140*, 221–224.

Patrick, R., Horin, C., Kobe, B., Cao, K.-A.L., and Bodén, M. (2016). Prediction of kinase-specific phosphorylation sites through an integrative model of protein context and sequence. Biochim. Biophys. Acta *1864*, 1599–1608.

Pickrell, A.M., and Youle, R.J. (2015). The Roles of PINK1, Parkin and Mitochondrial Fidelity in Parkinson's Disease. Neuron *85*, 257–273.

Princely Abudu, Y., Pankiv, S., Mathai, B.J., Håkon Lystad, A., Bindesbøll, C., Brenne, H.B., Yoke Wui Ng, M., Thiede, B., Yamamoto, A., Mutugi Nthiga, T., et al. (2019). NIPSNAP1 and NIPSNAP2 Act as "Eat Me" Signals for Mitophagy. Dev. Cell *49*, 509-525.e12.

Pugacheva, E.N., and Golemis, E.A. (2005). The focal adhesion scaffolding protein HEF1 regulates activation of the Aurora-A and Nek2 kinases at the centrosome. Nat. Cell Biol. *7*, 937–946.

Pugacheva, E.N., Jablonski, S.A., Hartman, T.R., Henske, E.P., and Golemis, E.A. (2007). HEF1-Dependent Aurora A Activation Induces Disassembly of the Primary Cilium. Cell *129*, 1351–1363.

Roghi, C., Giet, R., Uzbekov, R., Morin, N., Chartrain, I., Le Guellec, R., Couturier, A., Dorée, M., Philippe, M., and Prigent, C. (1998). The Xenopus protein kinase pEg2 associates with the centrosome in a cell cycle-dependent manner, binds to the spindle microtubules and is involved in bipolar mitotic spindle assembly. J. Cell Sci. *111 (Pt 5)*, 557–572.

Sasazawa, Y., Kanagaki, S., Tashiro, E., Nogawa, T., Muroi, M., Kondoh, Y., Osada, H., and Imoto, M. (2012). Xanthohumol Impairs Autophagosome Maturation through Direct Inhibition of Valosin-Containing Protein. ACS Chem. Biol. *7*, 892–900.

Schwarten, M., Mohrlüder, J., Ma, P., Stoldt, M., Thielmann, Y., Stangler, T., Hersch, N., Hoffmann, B., Merkel, R., and Willbold, D. (2009). Nix directly binds to GABARAP: A possible crosstalk between apoptosis and autophagy. Autophagy *5*, 690–698.

Sehdev, V., Katsha, A., Ecsedy, J., Zaika, A., Belkhiri, A., and El-Rifai, W. (2013). The combination of alisertib, an investigational Aurora kinase A inhibitor, and docetaxel promotes cell death and reduces tumor growth in preclinical cell models of upper gastrointestinal adenocarcinomas: Alisertib & Docetaxel Inhibit Tumor Growth. Cancer *119*, 904–914.

Sizaire, F., Le Marchand, G., Pécréaux, J., Bouchareb, O., and Tramier, M. (2020). Automated screening of AURKA activity based on a genetically encoded FRET biosensor using fluorescence lifetime imaging microscopy. Methods Appl. Fluoresc. *8*, 024006.

Tresse, E., Salomons, F.A., Vesa, J., Bott, L.C., Kimonis, V., Yao, T.-P., Dantuma, N.P., and Taylor, J.P. (2010). VCP/p97 is

essential for maturation of ubiquitin-containing autophagosomes and this function is impaired by mutations that cause IBMPFD. Autophagy *6*, 217–227.

Tsunematsu, T., Arakaki, R., Yamada, A., Ishimaru, N., and Kudo, Y. (2015). The Non-Canonical Role of Aurora-A in DNA Replication. Front. Oncol. *5*.

Twig, G., and Shirihai, O.S. (2011). The Interplay Between Mitochondrial Dynamics and Mitophagy. Antioxid. Redox Signal. *14*, 1939–1951.

Vaufrey, L., Balducci, C., Lafont, R., Prigent, C., and Le Bras, S. (2018). Size matters! Aurora A controls Drosophila larval development. Dev. Biol. *440*, 88–98.

Villa, E., Marchetti, S., and Ricci, J.-E. (2018). No Parkin Zone: Mitophagy without Parkin. Trends Cell Biol.

Walter, A.O., Seghezzi, W., Korver, W., Sheung, J., and Lees, E. (2000). The mitotic serine/threonine kinase Aurora2/AIK is regulated by phosphorylation and degradation. Oncogene *19*, 4906–4916.

Wang, H., Somers, G.W., Bashirullah, A., Heberlein, U., Yu, F., and Chia, W. (2006). Aurora-A acts as a tumor suppressor and regulates self-renewal of Drosophila neuroblasts. Genes Dev. *20*, 3453–3463.

Wei, Y., Chiang, W.-C., Sumpter, R., Mishra, P., and Levine, B. (2017). Prohibitin 2 Is an Inner Mitochondrial Membrane Mitophagy Receptor. Cell *168*, 224-238.e10.

Wirtz-Peitz, F., Nishimura, T., and Knoblich, J.A. (2008). Linking cell cycle to asymmetric division: Aurora-A phosphorylates the Par complex to regulate Numb localization. Cell *135*, 161–173.

Xian, H., Yang, Q., Xiao, L., Shen, H.-M., and Liou, Y.-C. (2019). STX17 dynamically regulated by Fis1 induces mitophagy via hierarchical macroautophagic mechanism. Nat. Commun. *10*, 2059.

Xue, Y., Zhou, F., Zhu, M., Ahmed, K., Chen, G., and Yao, X. (2005). GPS: a comprehensive www server for phosphorylation sites prediction. Nucleic Acids Res. *33*, W184–W187.

Yan, C., Gong, L., Chen, L., Xu, M., Abou-Hamdan, H., Tang, M., Désaubry, L., and Song, Z. (2019). PHB2 (prohibitin 2) promotes PINK1-PRKN/Parkin-dependent mitophagy by the PARL-PGAM5-PINK1 axis. Autophagy 1–16.

Yoshii, S.R., Kishi, C., Ishihara, N., and Mizushima, N. (2011). Parkin Mediates Proteasome-dependent Protein Degradation and Rupture of the Outer Mitochondrial Membrane♦. J. Biol. Chem. *286*, 19630–19640.

Yoshimaru, T., Komatsu, M., Tashiro, E., Imoto, M., Osada, H., Miyoshi, Y., Honda, J., Sasa, M., and Katagiri, T. (2015). Xanthohumol suppresses oestrogen-signalling in breast cancer through the inhibition of BIG3-PHB2 interactions. Sci. Rep. *4*, 7355.

Youle, R.J., and Narendra, D.P. (2011). Mechanisms of mitophagy. Nat. Rev. Mol. Cell Biol. *12*, 9–14.

Yu, X., Minter-Dykhouse, K., Malureanu, L., Zhao, W.-M., Zhang, D., Merkle, C.J., Ward, I.M., Saya, H., Fang, G., van Deursen, J., et al. (2005). Chfr is required for tumor suppression and Aurora A regulation. Nat. Genet. *37*, 401–406.

Zhang, J., Randall, M.S., Loyd, M.R., Dorsey, F.C., Kundu, M., Cleveland, J.L., and Ney, P.A. (2009). Mitochondrial clearance is regulated by Atg7-dependent and -independent mechanisms during reticulocyte maturation. Blood *114*, 157–164.

Zhang, Y., Ni, J., Huang, Q., Ren, W., Yu, L., and Zhao, S. (2007). Identification of the auto-inhibitory domains of Aurora-A kinase. Biochem. Biophys. Res. Commun. *357*, 347–352.

Zheng, F., Yue, C., Li, G., He, B., Cheng, W., Wang, X., Yan, M., Long, Z., Qiu, W., Yuan, Z., et al. (2016). Nuclear AURKA acquires kinase-independent transactivating function to enhance breast cancer stem cell phenotype. Nat. Commun. *7*, 10180.